Dalton Transactions

Nickel(II) Complexes with Covalently Attached Quinols Rely on Ligand-Derived Redox Couples to Catalyze Superoxide Dismutation

Journal:	*Dalton Transactions*
Manuscript ID	DT-ART-11-2024-003331
Article Type:	Paper
Date Submitted by the Author:	28-Nov-2024

Complete List of Authors:	Boothe, Robert; Auburn University Oppelt, Julian; Ludwig-Maximilians-Universität München Franke, Alicja; Ludwig-Maximilians-Universität München Moore, Jamonica; Auburn University Squarcina, Andrea; Ludwig-Maximilians-Universität München Zahl, Achim; Friedrich-Alexander-Universität Erlangen-Nürnberg Senft, Laura; Ludwig-Maximilians-Universität München Kellner, Ina; Ludwig-Maximilians-Universität München Awalah, Akudo; Auburn University Bradford, Alisabeth; Auburn University Obisesan, Segun; Auburn University Schwartz, Dean; Auburn University Ivanović- Burmazović, Ivana; Ludwig-Maximilians-Universität München Goldsmith, Christian; Auburn University

Nickel(II) Complexes with Covalently Attached Quinols Rely on Ligand-Derived Redox Couples to Catalyze Superoxide Dismutation

Robert Boothe,[†,a] Julian Oppelt,[‡,§,a] Alicja Franke,[‡,§] Jamonica L. Moore,[†] Andrea Squarcina,[‡] Achim Zahl,[§] Laura Senft,[‡] Ina Kellner,[‡] Akudo L. Awalah,[†] Alisabeth Bradford,[†] Segun V. Obisesan,[†] Dean D. Schwartz,[¥] Ivana Ivanović-Burmazović,[‡,*] and Christian R. Goldsmith[†,*]

[†]Department of Chemistry and Biochemistry, Auburn University, Auburn, AL 36849, USA
[‡]Department of Chemistry, Ludwig-Maximilians-Universität München, 81377 München, Germany
[§]Department of Chemistry and Pharmacy, Friedrich-Alexander-Universität Erlangen-Nürnberg, Egerlandster. 1, 91508 Erlangen, Germany
[¥]Department of Anatomy, Physiology, and Pharmacology, College of Veterinary Medicine, Auburn University, Auburn, AL 36849, USA

*Corresponding authors: Ivana.Ivanovic-Burmazovic@cup.uni-muenchen.de, crgoldsmith@auburn.edu

[a]These authors contributed equally to the manuscript.

Abstract

Although nickel is found in the active sites of a class of superoxide dismutase (SOD), nickel complexes with non-peptidic ligands normally do not catalyze superoxide degradation, and none has displayed activity comparable to those of the best manganese-containing SOD mimics. Here, we find that nickel complexes with polydentate quinol-containing ligands can exhibit catalytic activity comparable to those of the most efficient manganese-containing SOD mimics. The nickel complexes retain a significant portion of their activity in phosphate buffer and under operando conditions and rely on ligand-centered redox processes for catalysis. Although nickel SODs are known to cycle through Ni(II) and Ni(III) species during catalysis, cryo-mass spectrometry studies indicate that the nickel atoms in our catalysts remain the +2 oxidation state throughout SOD mimicry.

Introduction

The over-production of reactive oxygen species (ROS) has been linked to a wide array of cardiovascular,[1, 2] neurological,[3] and inflammatory disorders[4] as well as tumorigenesis.[5] Understanding when and where ROS concentrations spike during the progression of these pathologies could lead to improved ways to diagnose and treat these conditions. These potential benefits have motivated efforts by ourselves and others to develop redox-responsive probes capable of investigating the involvement of ROS in normal and aberrant physiology in conjunction with non-invasive magnetic resonance imaging (MRI) instrumentation.[6-14] The links between oxidative stress and the aforementioned health conditions have also motivated efforts to develop small molecule antioxidants that could potentially slow or even reverse disease progression. Many of these antioxidants are functional mimics of superoxide dismutases (SODs), which are enzymes that catalyze the degradation of $O_2^{\cdot -}$ to O_2 and H_2O_2 (Eq 1).[15-21]

Eq 1) $2\ O_2^{\cdot -} + 2\ H^+ \rightarrow O_2 + H_2O_2$

Our laboratories have developed and studied a series of Mn(II)-containing contrast agents for magnetic resonance imaging (MRI) that display changes to their T_1-weighted relaxivity (r_1) upon reaction with H_2O_2.[22-25] The more recent of these contrast agents feature ligands that contain quinol groups (Scheme 1).[23-25] Upon oxidation by H_2O_2, the quinols convert to *para*-quinones

(Scheme 2). The manganese complexes with both H_2qp1 and H_4qp2 were also found to be catalysts for $O_2^{\cdot-}$ decomposition, as assessed by the commonly used hypoxanthine/xanthine oxidase/lucigenin assay[26, 27] and subsequent stopped-flow kinetics analysis of the direct reactions between the compounds and superoxide.[24, 25, 28] Zn(II) complexes with H_2qp1 and H_4qp2 can also catalyze $O_2^{\cdot-}$ degradation, indicating that the redox activity of the ligand can allow even a redox-inactive metal ion to catalyze SOD-like reactivity.[29, 30] The quinolic ligands are inactive as catalysts in the absence of a bound metal ion.

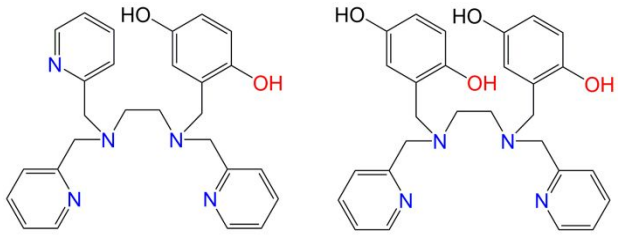

Scheme 1

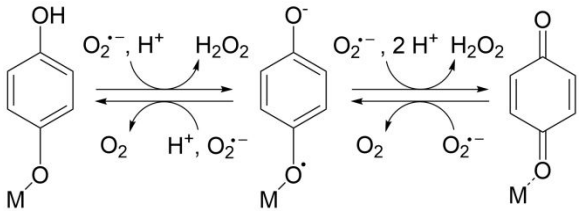

Scheme 2. Redox reactions involving quinols. This graphic was modified from one that appeared in reference [28].

The manganese and zinc SOD mimics prepared with quinolic ligands have provided two different sets of benefits. The Mn(II) complex with H_2qp1 is highly active in 4-(2-hydroxyethyl)-1-piperazineethanesulfonic acid (HEPES) buffer and appears to rely mostly on metal-centered redox processes for its SOD mimicry. Unfortunately, the catalyst loses over 90% of its activity in phosphate buffer. The Zn(II) complexes with H_2qp1 and H_4qp2, conversely, are more stable than their Mn(II) analogs but are less effective as SOD mimics in aqueous solutions with sulfonate-containing buffers.[29, 30] In phosphate solution, however, the Zn(II) complexes gain activity to the extent that they overtake their manganese analogs as catalysts under these conditions. That these Zn(II)-containing catalysts are not inhibited by phosphate is noteworthy since some non-

porphyrin-based manganese-based SOD mimics exhibit somewhat lower activity in phosphate buffer.[31-33] Given the high levels of phosphate in mammalian cells,[34, 35] this represents a substantial advantage for the Zn(II) complexes.

The use of Mn(II) poses a problem for both MRI and SOD mimicry in that this metal ion tends to bind to ligands more weakly than most other transition metal ions.[36, 37] The affinity of this metal ion for water is great enough to destabilize Mn(II) complexes with acyclic tetradentate linear ligands in aqueous solutions. When we partially oxidized the Mn(II)-H_4qp2 complex with H_2O_2, we measured a high aquation number that was difficult to rationalize unless at least some of the metal ion were released and complexed as $[Mn(H_2O)_6]^{2+}$.[25] Although "free" Mn(II) is not as toxic as unchelated iron or copper, it is nonetheless still harmful and has been documented to disrupt neurological function.[38] Most reported manganese-containing MRI contrast agents and SOD mimics have ligands that use macrocycles and/or a large number of anionic coordinating groups to stabilize the complex in water, but even these measures are not always sufficient to ensure suitably long-term stability.[20, 21, 39, 40] Such measures also pose severe constraints on the design and synthesis of manganese-containing MRI contrast agents and antioxidants.

The use of another transition metal ion could potentially relax these requirements due to the intrinsically greater complex stability.[37] The Zn(II) complexes demonstrate this as they are indeed more thermodynamically stable than their Mn(II) analogs.[28-30] The lack of redox activity for the metal, however, may limit the peak catalysis; without phosphate inhibition, the manganese compounds are more active. Ni(II) compounds generally have aqueous (thermodynamic) stabilities similar to Zn(II) complexes while displaying more extensive metal-centered redox activity and higher kinetic stability.[36] We initially decided to investigate Ni(II) complexes with H_2qp1 and H_4qp2 as redox-responsive MRI contrast agents that would operate through a chemical exchange saturation transfer (CEST) pathway involving bulk water exchanging ^{1}H nuclei with the quinolic OH groups.[41, 42] Although these complexes did not give rise to a practical and readily replicable CEST response to H_2O_2, we find both that the Ni(II)-for-Mn(II) substitution does indeed stabilize the complexes in water and that these compounds are potent antioxidants.

The use of nickel can heighten both the stability and activity of the SOD mimic. Unlike the zinc complexes, the activity is diminished by phosphate, but not to anywhere near the same extent as the Mn-H_2qp1 complex. The nickel complex with H_4qp2 is the more active of the two catalysts, and even with the inhibitory effect, it is a highly functioning SOD mimic in phosphate solution.

Mechanistically, the H_4qp2 complex with Ni(II) behaves like its Zn(II) analog in that it relies on ligand-centered redox for catalysis but appears to better resist decomposition.

Experimental Section

Materials

Most of the chemical precursors and solvents were bought from Sigma-Aldrich and used as received. 2,2-Diphenyl-1-picryl-hydrazyl hydrate (DPPH) was bought from EMD Millipore. All deuterated solvents were purchased from Cambridge Isotopes. Fisher supplied the diethyl ether (ether) and methanol (MeOH). Methylene chloride (CH_2Cl_2) was acquired from Mallinckrodt Baker. The ligands *N*-(2,5-dihydroxybenzyl)-*N,N',N'*-tris(2-pyridinylmethyl)-1,2-ethanediamine (H_2qp1) and *N,N'*-bis(2,5-dihydroxybenzyl)-*N,N'*-bis(2-pyridinylmethyl)-1,2-ethanediamine (H_4qp2) were prepared as previously described.[24, 25]

Instrumentation

All ^{1}H, ^{13}C, and ^{17}O NMR spectra were recorded on a 400 MHz AV Bruker NMR spectrometer. The ^{17}O NMR data were specifically collected on a Bruker AVANCE DRX 400WB spectrometer with a superconducting wide-bore magnet operating at a 54.24 MHz resonance frequency and a 9.4T magnetic induction. All reported NMR resonance peak frequencies were referenced to internal standards. Water exchange experiments involving **1** and **2** were performed in 60 mM MOPS, pH = 7.4 (+20% v/v MeCN) as well as in pure distilled water (+20% v/v MeCN). Neither **1** nor **2** exhibited significant broadening of the ^{17}O signal in either buffered or unbuffered water in comparison to the reference samples without the compounds. Optical data were collected on a Varian Cary 50 spectrophotometer and analyzed using software from the WinUV Analysis Suite. Electron paramagnetic resonance (EPR) spectra were collected using a Bruker EMX-6/1 X-band EPR spectrometer operated in perpendicular mode and analyzed with the program EasySpin. Each EPR sample was run as a frozen solution in a quartz tube. High-resolution mass spectrometry (HR-MS) data were obtained at the Mass Spectrometer Center at Auburn University on a Bruker microflex LT MALDI-TOF mass spectrometer via direct probe analysis operated in the positive ion mode. Infrared spectroscopy (IR) data were obtained with a Shimadzu IR Prestige-21 FT-IR spectrophotometer. A Johnson Matthey magnetic susceptibility balance (model MK I#7967) was used to measure the magnetic properties of the Ni(II) complexes; the reported μ_{eff} values are the average of two independent measurements, each of which corresponded to a unique solid sample.

Atlantic Microlabs (Norcross, GA) performed the elemental analyses (C, H, N). All samples submitted for elemental analysis were dried under vacuum prior to their shipment.

Cyclic voltammetry (CV) in aqueous solutions was performed using a Pine WaveDriver bipotentiostat using a 3 mm glassy carbon working electrode that was polished between each experiment, a Pt wire counter electrode, and a nonaqueous Ag^{+}/Ag pseudoreference electrode. Samples were analyzed in a 20 mL electrochemical glass cell with a Teflon cell top purchased from BASi Inc. Cyclic voltammetry measurements in MeCN were performed using an Autolab instrument with a PGSTAT 101 potentiostat. A three-electrode arrangement was employed consisting of a glassy carbon disk working electrode ($A = 0.07\ cm^2$) (Metrohm), a platinum counter electrode (Metrohm), and a silver wire (Metrohm) as reference electrode. Potentials were referenced to the redox couple of the internal standard $Fc^{+/0}$. Prior to each experiment, the electrode was polished with 1 μm alumina, rinsed with deionized water, and wiped with a paper tissue. All CV experiments were conducted at a scan rate of 100 mV/s at 293 K unless otherwise stated.

X-Ray Crystallography

Crystals were mounted in paratone oil on a glass fiber and aligned on a Bruker SMART APEX CCD X-ray diffractometer. Intensity measurements were performed using graphite monochromated Mo Kα radiation (λ = 0.71073 Å) from a sealed tube and monocapillary collimator. SMART (v 5.624) was used to determine the preliminary cell constants and regulate data acquisition. The intensities of reflections of a sphere were collected through the compilation of three sets of exposures (frames). Each set had a different ϕ angle for the crystal, with each exposure spanning a range of 0.3° in ω. A total of 1800 frames were collected with exposure times of 40 s per frame. The data were corrected for Lorentz and polarization effects. Structures were solved using direct methods and expanded using Fourier techniques. All non-hydrogen atoms were refined anisotropically. Hydrogen atoms were included at idealized positions 0.95 Å from their parent atoms prior to the final refinement. Further details regarding the data acquisition and analysis are included in Tables 1 and 2.

Potentiometric Titrations

The speciation chemistry of the Ni(II) complexes in water was probed using a METROHM 765 Dosimat with a jacketed, airtight glass titration vessel. A Fisher Scientific Accumet Research AR15 pH meter was used to determine the pH of the sample solutions during the titrations. The electrode was calibrated before each titration using commercially available standard solutions

buffered to pH 4.0, 7.0, and 10.0. All samples were purged with argon prior to analysis and subsequently analyzed under an argon atmosphere at 25 °C. All solution samples were prepared in solutions of 100 mM KCl in deionized Millipore water. The titrations investigating metal-ligand speciation were run with solutions that contained a 1:1 molar mixture of the ligand and $Ni(OTf)_2$. Carbonate-free solutions of 0.10 M KOH and 0.10 M HCl were prepared using argon-saturated deionized Millipore water. We attempted to analyze and fit the data to speciation models using the Hyperquad2006 software.[43]

Analysis of the Antioxidant Properties of the Coordination Complexes

We initially assessed the antioxidant activities of the Ni(II) complexes through the DPPH assay (DPPH = 2,2-diphenyl-1-picrylhydrazyl radical hydrate).[44-46] In this assay, potential antioxidants are tested for their abilities to donate hydrogen atoms to the radical to generate the corresponding hydrazine. Aqueous solutions of either **1**, **2**, or ascorbic acid were added to a solution of 0.10 mM DPPH in MeOH, such that the final reaction volume was 0.2 mL. Samples were incubated in the dark for 30 min at room temperature (RT) before being spectrophotometrically analyzed on a Molecular Devices Spectramax Plus spectrophotometer. The absorbance at 517 nm, the λ_{max} of the hydrazine product, was recorded. Experiments were performed in triplicate.

Determination of in vitro *SOD Activity via Stopped-Flow Techniques*

The ability of **1** and **2** to catalytically degrade superoxide was assessed by a direct method using stopped-flow techniques that has been more fully described in prior work from one of our laboratories.[31] Stopped-flow measurements were performed on a Biologic SFM-400 four syringe stopped-flow system using only the first three syringes and a Berger Ball mixer to minimize mixing effects between aqueous buffered solutions and DMSO solutions of KO_2. A J&M TIDAS S MMS UV/VIS diode array detector (integration time 0.5 ms, 180 nm – 720 nm wavelength) and an Energetiq LDLS ENQ EQ-99-FC laser driven light source were used.

Superoxide solutions were prepared by suspending 220 – 240 mg KO_2 in 20 mL dry DMSO. The suspension was stirred for at least 30 min under inert atmosphere before the suspension was filtered through a PTFE syringe filter (Ø = 0.45 μm) to give a saturated KO_2 solution, which was transferred to the stopped-flow setup. The potential SOD mimics (SODm) were dissolved in aqueous solutions buffered to either pH 7.4 or 7.8. The buffers were prepared from Millipore water and either 4-morpholinepropanesulfonic acid (MOPS) or sodium dihydrogen

phosphate. The concentration of the buffer was 60 mM, and the ionic strength was adjusted to 150 mM for each solution through the addition of NaCl. Prior to use, all buffered solutions were treated with Chelex 100 sodium exchange resin for at least 24 h to remove adventitious metal ions. Stock solutions containing 0.10 mM M of each tested SODm were prepared in each buffer; if necessary, the stock solution contained 10% DMSO to ensure that the complexes dissolved fully. The stock solutions were diluted in buffer to give a series of SODm concentrations suitable for the stopped-flow experiments.

Kinetic measurements were performed adding a large excess of superoxide to the putative SOD mimetic: $[O_2^{\cdot -}] = 100 – 200$ μM, [SODm] = 0.045 – 4.5 μM. The aqueous solution containing the studied Ni(II) complex was mixed in a 9:1 ratio with the superoxide solution in DMSO using a high-density mixer. In each experiment, the concentration of superoxide exceeded that of the nickel-containing catalyst by at least ten-fold to ensure catalytic conditions. All kinetic data were fit with the program Biokine 32 V4.80. Each presented k_{obs} value represents an average of at least ten measurements. Each k_{cat} was determined from the slope of k_{obs} vs. [SODm]. All measurements were performed at 21 °C.

Cryospray-Ionization Mass Spectrometry

Cryospray-ionization mass spectrometry (CSI-MS) measurements were performed on a UHR-TOF Bruker Daltonik maXis Plus, an ESI-quadrupole time-of-flight (qToF) mass spectrometer capable of a resolution of at least 60.000 (FWHM), which was coupled to a Bruker Daltonik Cryospray unit. The detector was run in positive ion mode with a source voltage of 3.5 kV and a flow rate of 240 μL/h. The temperatures of the N_2 spray gas and the dry gas used for solvent removal were -40 °C. The mass spectrometer was calibrated prior to each experiment *via* direct infusion of an Agilent ESI-TOF low concentration tuning mixture, which provided a m/z range of singly charged peaks up to 2700 Da in both ion modes. For the reactions with $O_2^{\cdot -}$, 1×10^{-5} M solutions of each compound in MeCN were cooled to -40 °C and mixed with excess solid KO_2. Aliquots from the resultant mixtures were then injected into the mass spectrometer. To ensure the survival of metastable reaction species generated at low temperatures, the injection syringe and the tubing of the mass spectrometer were precooled with -40 °C solvent. After tempering, the reaction solutions were injected as quickly as possible, with the recording of mass spectrometry data commencing immediately afterwards. Multiple samples were collected and analyzed over time to determine whether the product distribution was changing during the reaction. Aliquots

were also analyzed after the reactions warmed to RT. The solvents were not rigorously dried to ensure a source of protons. The measured data were processed and analyzed with Bruker Data Analysis 5.2.

Syntheses

Acetonitrilo(*N*-(2,5-Dihydroxybenzyl)-*N,N',N'*-tris(2-pyridinylmethyl)-1,2-ethanediamine) nickel(II) triflate ([Ni(H_2qp1)(MeCN)]($OTf)_2$, 1).

The H_2qp1 ligand (105 mg, 0.230 mmol) and nickel(II) triflate ($Ni(OTf)_2$, 83 mg, 0.23 mmol) were dissolved in 3 mL of acetonitrile (MeCN) under air. The solution was stirred for 30 min at RT. The solvent was removed to yield an oily reddish solid. The crude was recrystallized from a mixture of MeCN and ether to yield the product as dark red crystals that were suitable for single crystal X-ray diffraction (179 mg, 89%). ^{1}H NMR (500 MHz, CD_3CN, 294 K): 51.9, 45.9, 15.2, 14.4, 8.8, 6.7 (quinol O-H), 4.9, 3.3. Optical spectroscopy (MeOH): 255 nm (6800 M^{-1} cm^{-1}), 299 nm (3430 M^{-1} cm^{-1}), 444 nm (285 M^{-1} cm^{-1}), 504 nm (195 M^{-1} cm^{-1}), 674 (150 M^{-1} cm^{-1}). Solid-state magnetic susceptibility (294 K): μ_{eff} = 3.4 μ_B. IR (KBr, cm^{-1}): 3529 (s), 3289 (s), 2286 (m), 1608 (s), 1574 (m), 1463 (s), 1364 (m), 1278 (s), 1256 (s), 1226 (s), 1158 (s), 1073 (w), 1056 (w), 1029 (s), 949 (w), 824 (m), 766 (s), 730 (w), 639 (s), 573 (w), 517 (m), 429 (w). CV (100 mM phosphate buffer, pH 7.2, 100 mV/s): E_{pa} = 60 mV vs. Ag/AgCl, E_{pc} = 0 mV vs. Ag/AgCl. Elemental analysis (crystals): Calcd for $C_{31}H_{32}N_6F_6O_8S_2Ni•2H_2O$: C, 41.86%; H, 4.08%; N, 9.45%; Found: C, 41.76%; H, 3.91%; N, 9.38%.

***cis*-Diacetonitrilo(*N,N'*-bis(2,5-dihydroxybenzyl)-*N,N'*-bis(2-pyridinylmethyl)-1,2-ethanediamine)nickel(II) triflate ([Ni(H_4qp2)($MeCN)_2$]($OTf)_2$, 2).**

The H_4qp2 ligand (152 mg, 0.312 mmol) and $Ni(OTf)_2$ (114 mg, 0.319 mmol) were dissolved in 3 mL of MeCN under N_2. The solution was stirred for 30 min at RT. Ether was gradually added to the reaction mixture to yield large, purple crystals of the product that were suitable for single crystal X-ray diffraction (95 mg, 42%). ^{1}H NMR (400 MHz, CD_3CN, 294 K): 54.9, 41.2, 16.7, 9.7, 6.7 (quinol O-H), 4.9, 3.3. Optical spectroscopy (MeCN): 298 nm (7550 M^{-1} cm^{-1}), 438 nm (610 M^{-1} cm^{-1}), 493 nm (380 M^{-1} cm^{-1}), 668 (130 M^{-1} cm^{-1}). Solid-state magnetic susceptibility (294 K): μ_{eff} = 3.4 μ_B. IR (KBr, cm^{-1}): 3371 (s), 1610 (s), 1574 (m), 1509 (s), 1454 (s), 1252 (s), 1201 (s), 1173 (s), 1107 (w), 1029 (s), 948 (w), 879 (w), 818 (m), 761 (s), 729 (w), 639 (s), 578 (w), 519 (m), 422 (m). CV (100 mM phosphate buffer, pH 7.2, 100 mV/s): E_{pa} = 170 vs. Ag/AgCl, E_{pc} = -140 mV vs. Ag/AgCl, -670 mV vs. Ag/AgCl. Elemental analysis: Calcd for

$C_{34}H_{36}N_6F_6O_{10}S_2Ni•2.0H_2O$ C, 42.47%; H, 4.19%; N, 8.74%; Found: C, 42.13%; H, 3.98%; N, 8.32%.

Results

Synthesis and Characterization

The syntheses of the Ni(II) complexes are facile, and both complexes form upon simply mixing the ligand and $Ni^{II}(OTf)_2$ in MeCN under N_2. Pure $[Ni^{II}(H_2qp1)(MeCN)](OTf)_2$ (**1**) and $[Ni^{II}(H_4qp2)(MeCN)_2](OTf)_2$ (**2**) can be crystallized in approximately 90% and 40% yields, respectively. The yield of **2** is substantially lower than the 75% value typically found for $[Mn^{II}(H_4qp2)Br_2]$.[25] We speculate that the greater solubility of **2** in MeCN reduces the amount of material that we can cleanly precipitate and crystallize from this solvent. Elemental analysis indicates that both **1** and **2** are hygroscopic, which was also observed for the Mn(II) complex with H_2qp1 and the Zn(II) complex with H_4qp2.[24, 30]

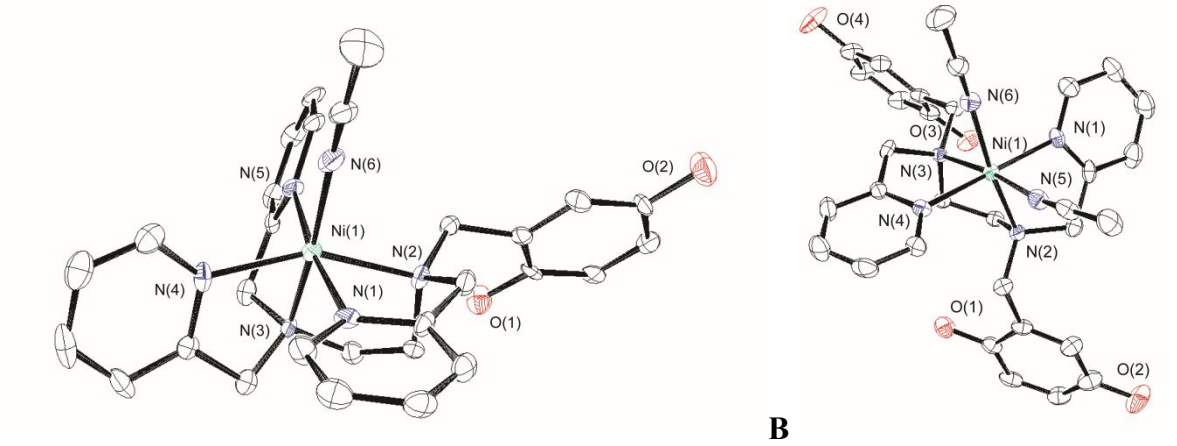

A **B**

Figure 1. ORTEP representations of A) $[Ni(H_2qp1)(MeCN)]^{2+}$ (**1**) and B) $[Ni(H_4qp2)(MeCN)_2]^{2+}$ (**2**). All hydrogen atoms, triflate counteranions, and solvent molecules have been removed for clarity. All ellipsoids are at 50% probability. Full crystallographic data are provided in the ESI and in the Cambridge Structural Database (numbers 2390972 and 2390973).

The nickel remains in the +2 oxidation state upon complexation by either quinol-containing ligand. For both **1** and **2**, the solid-state magnetic susceptibility measurements are consistent with μ_{eff} values of 3.4 μ_B; these are in the middle of the 2.8-4.0 μ_B range reported for previously characterized Ni(II) complexes.[47] The complexes are both EPR-silent but display paramagnetic ^1H NMR spectra (Figure S1, Figure S2); these spectroscopic characteristics are likewise consistent with the assignment of S = 1 metal centers. Upon adding D_2O to the NMR samples, the peaks at

6.7 ppm decrease in intensity for both **1** and **2**, leading us to assign these to quinolic O-H resonances. The complexes were also characterized by IR and UV/vis (Figures S3-S5). In MeCN, both Ni(II) complexes display bands around 300 nm; we have observed similar features for other metal complexes with polydentate quinol-containing ligands.[23-25, 29, 30, 48-50]

Table 1. Selected crystallographic data for **1** and **2**

Parameter	$[Ni(H_2qp1)(MeCN)](OTf)_2$ (**1**)	$[Ni(H_4qp2)(MeCN)_2](OTf)_2$ (**2**)
Formula	$C_{31}H_{34}F_6N_6NiO_9S_2$	$C_{38}H_{42}F_6N_8NiO_{10}S_2$
MW	871.47	1007.62
Crystal system	Orthorhombic	Orthorhombic
Space group	*Pca2₁*	*P2₁2₁2₁*
a (Å)	16.662(2)	12.8113(6)
b (Å)	12.3619(16)	17.4024(9)
c (Å)	17.649(2)	20.1442(10)
α (°)	90	90
β (°)	90	90
γ (°)	90	90
V (Å^3)	3635.2(8)	4491(4)
Z	4	4
Crystal color	Clear light purple	Clear violet
T (K)	180	180
Reflns collected	29809	105753
Unique reflns	3992	9748
R1 (F, I > 2σ(I))	0.0620	0.0730
wR2 (F^2, all data)	0.1175	0.1496

$R1 = \Sigma \left| |F_o| - |F_c| \right| / \Sigma |F_o|$; $wR2 = [\Sigma w(F_o^2-F_c^2)^2/\Sigma w(F_o^2)^2]^{1/2}$.

Complexes **1** and **2** are readily crystallized from mixtures of MeCN and ether (Table 1). The crystal structures show that the H_2qp1 and H_4qp2 ligands are bound to the metal center in pentadentate and tetradentate fashions, respectively, through their amine and pyridine groups (Figure 1). None of the quinols are bound to the Ni(II) in either structure. Each Ni(II) center is coordinated by a distorted octahedral array of donor atoms consisting of the N-donors from the polydentate ligands and either one (**1**) or two (**2**) MeCN molecules occupying the remaining coordination sites. The metal-ligand bond distances corroborate the assignment of +2 oxidation states for the nickel ions (Table 2).[51] The C-O bond distances average 1.37 Å, demonstrating that the quinols remain both protonated and in their reduced states.[24, 52]

Table 2. Selected bond lengths (Å) for complexes **1** and **2**

Complex	**1**	**2**
Ni-N(1)	2.150(7)	2.079(3)
Ni-N(2)	2.140(8)	2.125(3)
Ni-N(3)	2.101(7)	2.137(4)
Ni-N(4)	2.077(8)	2.078(3)
Ni-N(5)	2.100(8)	2.110(4)
Ni-N(6)	2.062(8)	2.067(4)
C-O(1)	1.369(11)	1.369(6)
C-O(2)	1.381(12)	1.370(6)
C-O(3)		1.375(6)
C-O(4)		1.372(7)

N(1) and N(4) correspond to pyridine nitrogens; N(2) and N(3) correspond to amine nitrogens; N(6) corresponds to a MeCN nitrogen. N(5) corresponds to a pyridine nitrogen for **1** and a MeCN nitrogen in **2**. The atoms in **1** and **2** have been relabeled to facilitate comparisons between the structures.

Characterization of the Aqueous Chemistry of the Ni(II) Complexes

Potentiometric pH titration data suggest that the quinols readily deprotonate and bind to the Ni(II) centers in anaerobic aqueous solutions, contrary to what is observed in the crystal structures (Figure S6). The H_2qp1 ligand by itself was previously found to undergo two ionization events with pK_a values of 4.72 and 7.24;[29] these are consistent with the protonation of a pyridine ring and the tertiary amines, respectively.[36] Due to the previously observed precipitation of the ligands under basic and metal-free conditions, we were unable to measure the pK_a values of the O-H protons; these are estimated to be about 10, the pK_a value for free 1,4-hydroquinone.[53] Intramolecular hydrogen bonding was observed in the crystal structure of the ligand, which we believe renders it unavailable for further protonation.[29]

Our best fits of the data collected for **1** suggest that free ligand is not present to an appreciable degree between pH 2.5 and 9.0. Since we do not observe dissociation of the ligand, we cannot calculate formation constants for either $[Ni(Hqp1)]^+$ or $[Ni(H_2qp1)]^{2+}$, where $Hqp1^-$ is the singly deprotonated form of the ligand. We observe an ionization event consistent with a pK_a value of 6.33 (±0.05), which is assigned to the deprotonation of a Ni(II)-bound quinol as the pH is increased.[9, 54, 55] The ionization event is replicated upon reacidification of the basic end-solution

(Figure S6). Consequently, we believe that the predominant species between pH 7.0 and 7.4 is $[Ni(Hqp1)]^+$.

The Ni(II) complex with H_4qp2 also appears to be stable in water, and the lack of free ligand under even the most acidic of the tested conditions again precluded us from calculating accurate stability constants. The H_4qp2 ligand was previously observed to display two ionization events upon either basification of an acidic solution or acidification of a basic solution. The corresponding pK_a values of 4.47 and 7.18 were assigned to the (de)protonation events involving a pyridine and tertiary amine, respectively.[25] When **2** is subjected to the same conditions, we observe two clear ionization events between pH 3 and 10. The corresponding pK_a values of 5.99 (±0.05) and 8.24 (±0.05) are assigned to the sequential deprotonation of metal-bound quinols as pH is increased. Consequently, we believe that the complex is predominantly $[Ni(H_3qp2)]^+$ between pH 7.0 and 7.4, with H_3qp2^- being the singly deprotonated form of the ligand. As was found in MeCN solution, the ^{1}H NMR spectra of the Ni(II) complexes in 20% MeCN/80% water are consistent with paramagnetic metal centers (Figure S1, Figure S2). Overall, the data indicate that the ligands fully coordinate the metal centers of both **1** and **2** in water.

The species assignments are supported by spectrophotometric pH titrations in aqueous solutions (Figure S7). The UV/vis spectra of both **1** and **2** at pH 7.0 feature bands at 313 nm, consistent with metal-bound quinolate ligands.[25] Upon acidification, these bands disappear and new peaks appear at 294 and 293 nm for **1** and **2**, respectively. Similar changes were observed for the protonation of $[Mn(H_3qp2)]^+$ and $[Zn(Hqp1)]^+$ in water.[25, 29] Given the noted tendency of Ni(II) to avoid heptacoordination, even transiently as an intermediate in ligand exchange,[56, 57] it is unlikely that water molecules are directly coordinated to the metal center in **1** when it is dissolved in water. Since the quinols are relatively poor ligands for metal ions, a water molecule could conceivably enter the coordination sphere in **2**, yielding $[Ni(H_3qp2)(H_2O)]^+$.

^{17}O NMR measurements of the complexes in the presence of ^{17}O-labeled water, however, indicate that rapid water molecule exchange does not occur on the metal centers of either **1** or **2**. Water exchange kinetics were probed in 60 mM MOPS buffered to pH 7.4 and buffer-free distilled water, with 20% v/v MeCN added to solubilize the coordination complexes in both types of aqueous solutions. Samples containing **1** or **2** do not display broadened ^{17}O NMR signals relative to the nickel-free standards. Since the complexes remain paramagnetic in water (Figure S1, Figure

S2), the data are consistent with negligible water molecule exchange between the Ni(II) centers and the bulk solvent.

Electrochemical Behavior

Both **1** and **2** were analyzed by cyclic voltammetry (CV) in 100 mM phosphate solution buffered to pH 7.2 (Figure 2, Table 3). Each nickel complex displays a redox feature with an $E_{1/2}$ between 15 and 30 mV vs. Ag/AgCl. Redox events with similar $E_{1/2}$ values were observed for Mn(II) and Zn(II) complexes with H_2qp1 and H_4qp2 (Table 3), leading us to assign these features to the oxidation and reduction of the quinolic portions of the organic ligands.[24, 25, 29, 30] The currents for **2** are approximately double of those for **1**. This further supports their assignment to ligand-derived redox processes since **2** has two quinols versus the single quinol for **1**. As assessed by the ΔE values measured with a 100 mV/s scan rate, the ligand oxidation for **1** is reversible, whereas that for **2** is irreversible. The ΔE for manganese and zinc complexes with H_4qp2 were likewise much greater than their H_2qp1 analogs.[24, 25, 29, 30] Notably, no higher potential oxidations are observed for **1** and **2**. With the manganese analogs, conversely, we detected peaks consistent with the oxidation of Mn(II) to Mn(III).[24, 25] For complex **2**, we observe an additional reduction with E_{pc} = -670 vs. Ag/AgCl.

Table 3. Summary of electrochemical data for ligand-associated redox processes of H_2qp1 and H_4qp2 complexes.

Complex	$E_{1/2}$ (mV)	ΔE (mV)	Reference
Ni-H_2qp1 (**1**)	29	59	This work
Mn-H_2qp1	115	135	[24]
Zn-H_2qp1	110	95	[29]
Ni-H_4qp2 (**2**)	15	310	This work
Mn-H_4qp2	57	232	[25]
Zn-H_4qp2	195	208	[30]

All CV was done in 100 mM phosphate solution buffered to pH 7.2 with a 100 mV/s scan rate.

Analysis of the nickel complexes in MeCN likewise fail to detect oxidation of the metal to Ni(III) (Figures S8-S11). The data differ from those collected in buffered water in that the redox processes associated with the oxidation of the quinol to the semiquinone are highly irreversible, likely due to subsequent deprotonation of the oxidized form of the ligand. Upon adding triethylamine, these features shift to lower potentials and become much more reversible, supporting our hypothesis that the irreversibility results from acid/base reactions that occur after redox. For both **1** and **2**, we observe currents corresponding to the oxidation of the quinol to

semiquinone and its subsequent reduction. For **1**, we also detect quasi-reversible features consistent with the oxidation of the semiquinone to the *para*-quinone and its subsequent reduction. As with the aqueous data, the magnitude of the currents for **2** are approximately twice those for **1**, supporting the assignment of the redox events to ligand- rather than metal-derived processes.

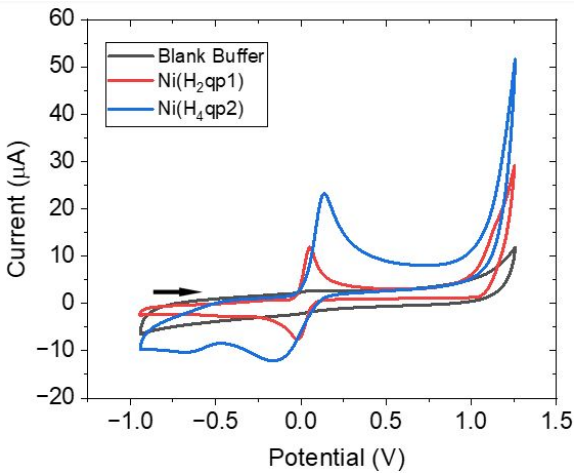

Figure 2. Cyclic voltammetry of 1.0 mM solutions of **1** (red) and **2** (blue) in water containing 100 mM phosphate buffered to pH 7.2. Data for nickel-free phosphate buffer (black) are provided for comparative purposes. The reference electrode was Ag/AgCl. The scan rate for all three sets of data was 100 mV/s. The arrow indicates the starting potential and initial scan direction. Complex **1** has $E_{1/2}$ = 29 mV vs. Ag/AgCl (ΔE = 59 mV). Complex **2** has $E_{1/2}$ = 15 mV vs. Ag/AgCl (ΔE = 310 mV).

Antioxidant Activity

We attempted to screen **1** and **2** for antioxidant activity using two common assays. The xanthine oxidase/hypoxathine/lucigenin assay is frequently used to probe the ability of an antioxidant to decompose superoxide.[24-27] Unfortunately, we were unable to obtain reliable data from this method. We believe that the photophysical properties of the Ni(II) complexes obfuscate the analysis. Lucigenin needs to absorb light at 460 nm to produce a chemiluminescent signal, but both **1** and **2** absorb strongly in this region as well.

The DPPH assay tests the ability of antioxidants to donate hydrogen atoms to 2,2-diphenyl-1-picrylhydrazyl radical hydrate (DPPH).[44-46, 58] Hydrogen atom transfer to DPPH yields a distinctly colored hydrazine product which can be identified and quantified by UV/vis. Both **1** and **2** are strong antioxidants by this measure, with 12.5 μM (**1**) and 6.3 μM (**2**) being sufficient to convert half the radical to the hydrazine (Figure S12). 21.9 μM of ascorbic acid was needed to

elicit a similar response. Other divalent metal complexes with the H_2qp1 and H_4qp2 ligands likewise outperformed ascorbic acid in these measurements by approximately the same extent.[24, 25, 29] The high sensitivity of the DPPH assay precludes us from drawing more quantitative conclusions regarding the relative reactivities of the H_2qp1 and H_4qp2 complexes.

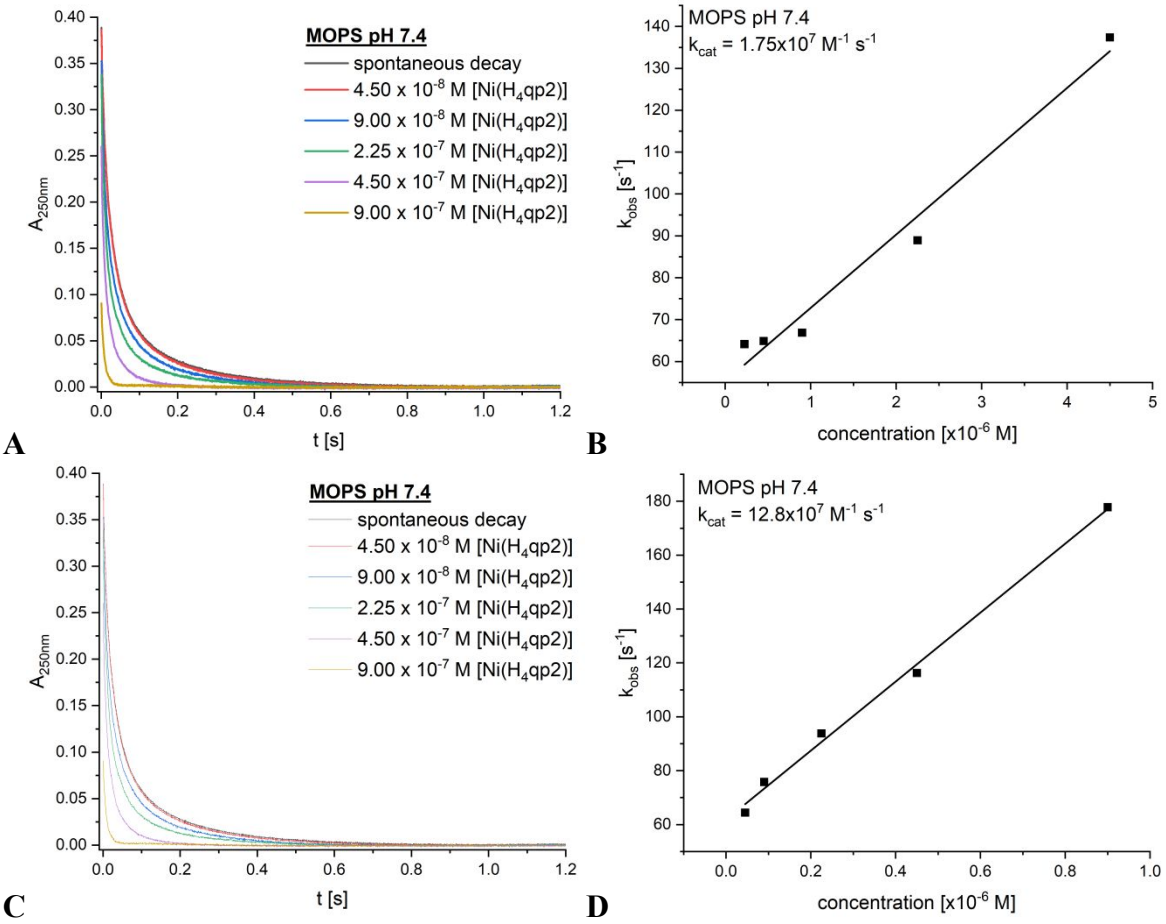

Figure 3. Kinetic traces and k_{obs} vs. concentration plots for nickel-catalyzed superoxide decomposition. The data were taken in 60 mM MOPS buffered to pH 7.4. The absorbance at 250 nm was followed. Each trace is labelled with the concentration of added Ni(II) complex. A) Kinetic traces for **1**. B) Plot of k_{obs} vs. [**1**]. C) Kinetic traces for **2**. D) Plot of k_{obs} vs. [**2**].

Table 4. Catalytic rate constants, k_{cat} (M^{-1} s^{-1}), measured by stopped-flow kinetics for the direct reactions of **1** and **2** with superoxide.

Buffer, pH	**1** (Ni-H_2qp1)	**2** (Ni-H_4qp2)	Mn-H_2qp1	Mn-H_4qp2	Zn-H_2qp1	Zn-H_4qp2
60 mM MOPS, 7.4	1.75×10^7	12.8×10^7	9.7×10^7 [a]	1.2×10^7 [a]	3.4×10^6 [b]	1.56×10^7 [c]
60 mM MOPS, 7.8	1.18×10^7	9.74×10^7				4.94×10^7 [c]
50 mM Phosphate, 7.4	1.08×10^7	6.21×10^7	8.0×10^6 [a]	1.0×10^7 [a]	1.9×10^7 [b]	2.54×10^7 [c]

[a]Data from reference [28]. 60 mM HEPES used instead of MOPS. [b]Data from reference [29]. 60 mM HEPES used instead of MOPS. [c]Data from reference [30].

The aforementioned assays are imperfect measures of the actual reactivity with $O_2^{\cdot-}$ due to the possibility of competing side-reactions between the various components in the reaction mixtures.[19, 31, 59-62] We more thoroughly and accurately gauged the antioxidant activity by following the direct reactions between the Ni(II) compounds and KO_2 with stopped-flow kinetics methods. These studies confirm that both **1** and **2** are highly capable SOD mimics (Figure 3, Table 4, Figures S13-S16). $O_2^{\cdot-}$ spontaneously dismutates without a catalyst; the rate law for this background reactivity is second-order in [$O_2^{\cdot-}$]. The metal-free H_2qp1 and H_4qp2 ligands were previously found to be incapable of catalyzing superoxide degradation.[28, 29] With either **1** or **2**, however, the decay rate instead becomes first-order in [$O_2^{\cdot-}$]. Varying the amount of catalyst reveals that the rate also has a first-order dependence on the concentration of the nickel complex, consistent with the catalyst and $O_2^{\cdot-}$ reacting in the rate-determining step. The H_4qp2 complex is the more active of the two in all three studied aqueous media by approximately six- to eight-fold. The activity is highest in MOPS buffered to pH 7.4 and lowest in pH 7.4 phosphate solutions. Approximately half of the activity is lost going from MOPS to phosphate buffer.

Mass Spectrometry Analysis of Intermediates and End-Products

The activity between the Ni(II) complexes and excess KO_2 in MeCN was probed by CSI-MS at -40 °C (Figure 4, Figures S17-S22). Without any KO_2, the quinols and metal center of **2** remain in their reduced forms: $[Ni^{II}(H_4qp2)]^{2+}$ and its conjugate base $[Ni^{II}(H_3qp2)]^{+}$ (Figure S17). With **1**, conversely, we detect traces of $[Ni^{II}(qp1)]^{2+}$, where *qp1* is the *para*-quinone form of the ligand (Scheme 3), even in the absence of oxidant (Figure S18). Within 1 min after the addition of KO_2, we detect Ni(II) species with two-electron oxidized mono-*para*-quinone forms of the ligands (*qp1*, H_2qp2, and $Hqp2^-$) for both **1** and **2** (Figure 4). We also find traces of oxygenated ligands. The data support the formation of Ni(II) complexes with semiquinone ligands. For **1**, a m/z peak at 511.1513 is consistent with $[Ni(qp1^{\bullet})]^{+}$, where the ligand is $qp1^{-\bullet}$. For **2**, m/z peaks at 271.5766 and 270.5687 can be assigned to $[Ni^{II}(H_3qp2^{\bullet})]^{2+}$ and $[Ni^{II}(Hqp2^{\bullet})]^{2+}$, which feature $H_3qp2^{\bullet}$ and the mono-*para*-quinone $Hqp2^{\bullet}$, respectively. We observe neither the di-*para*-quinone form of the ligand, *qp2* (Scheme 3), nor its Ni(II) complex at 1 min. After 5 min, m/z peaks consistent with the loss of the quinol arm for **1** appear (Figure S19), but this sort of degradation is not observed for **2** (Figure S20), suggesting that this compound is more oxidatively robust.

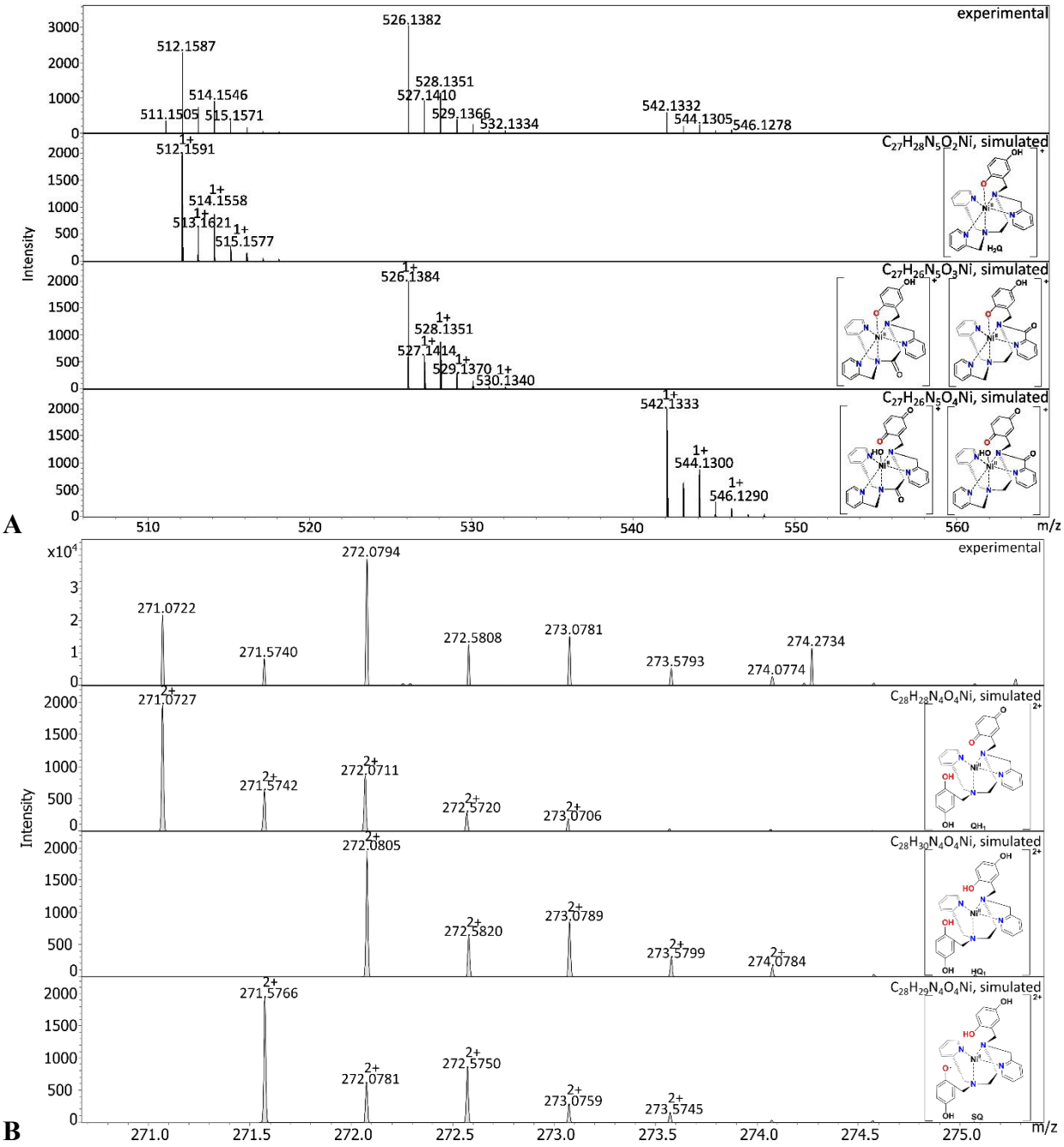

Figure 4. CSI-MS spectrometry of A) **1** and B) **2** after a 1 min reaction with KO_2. The graphics depict possible structures; we cannot preclude other modes of ligand coordination or sites of ligand oxidation. Experimental conditions: 1 mM solutions of each Ni(II) complex in MeCN (1% DMF) were cooled to -40 °C and then mixed with an excess of solid KO_2. Subsequently, the mixture was diluted in a pre-cooled syringe with pre-cooled MeCN to approximately 1×10^{-5} M and quickly injected into the mass spectrometer 1 min after the start of the reaction.

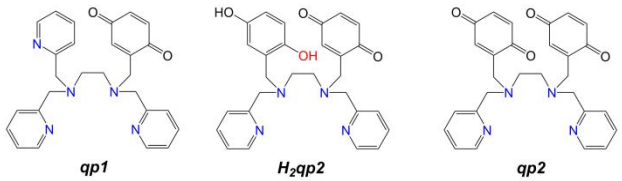

Scheme 3. Oxidized versions of the H_2qp1 and H_4qp2 ligands. Oxidized forms of the ligand are denoted by italics throughout the manuscript.

The Ni(II) compounds and their Zn(II) analogs differ substantially when the reaction aliquots are warmed to RT before MS analysis. Compound **1** appears to completely degrade (Figure S21), but the m/z peaks observed for **2** are consistent with Ni(II) complexes with oxidized forms of the ligands (Figures S22). These initially include the mono-*para*-quinone *H_2qp2* itself and singly and doubly oxygenated forms of both *H_2qp2* and H_4qp2. That some of the dioxygenated ligands contain quinols may suggest that the *para*-quinones are still capable of cycling back to the quinol oxidation state even after other portions of the ligand have been oxidized. When we warmed solutions of $[Zn^{II}(H_4qp2)]^{2+}$ and KO_2 to RT before analysis, we instead observe metal-free oxidized ligands rather than Zn(II) complexes.[30]

Low-Temperature UV/vis Analysis

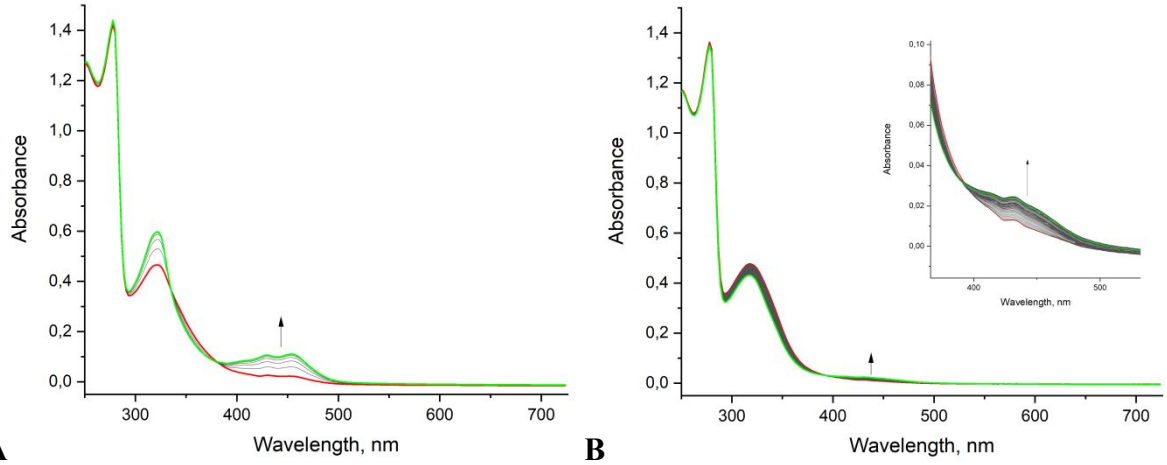

Figure 5. UV/vis data for the -40 °C MeCN reactions between excess KO_2 and A) 0.1 mM **1** and B) 0.1 mM **2**. Data were acquired with a 1.0 cm pathlength.

The proposed semiquinone intermediates are corroborated by UV/vis measurements taken at -40 °C (Figure 5). The reaction between **1** and KO_2 results in the formation of bands at 430 and 454 nm. Much smaller bands at 430 and 448 nm develop during analogous reactions with **2**. The

energies of these features are close to those of the 422 and 448 nm bands seen for manganese and zinc complexes with the semiquinone forms of these ligands[28, 30] as well as those of semiquinone radical by itself.[63, 64] The manganese and zinc complexes with H_4qp2 were previously found to give rise to features at 520 that are consistent with quinhydrone species,[28, 30] but we unable to unambiguously detect a similar feature for **2**.

Operando Stability of the Ni(II)-H_4qp2 Catalyst

The CSI-MS experiments failed to detect metal-free oxidized ligands in the reactions between **2** and KO_2, suggesting that **2** does not release its metal ion upon reaction with KO_2 and subsequent warming to RT. The Zn(II) analog of **2**, $[Zn^{II}(H_4qp2)]^{2+}$, does release the metal ion as the ligand is oxidized.[30] We took the resultant solutions for **2** and $[Zn^{II}(H_4qp2)]^{2+}$ and added fresh KO_2 from a 0.5-1.0 mM stock solution to determine whether the metal-containing products were still viable SOD mimetics. The activity of the nickel complex remains high, whereas that for the zinc is almost completely eliminated (Figure 6). For **2**, a 0.9 μM solution that was treated with 9 μM KO_2 retains 89% of its initial activity. Even with a much larger 120 μM KO_2 pre-treatment, **2** is 43% as active as a fresh batch. With $[Zn^{II}(H_4qp2)]^{2+}$, on the other hand, a two-fold excess of KO_2 is sufficient to eliminate 39% of the activity.

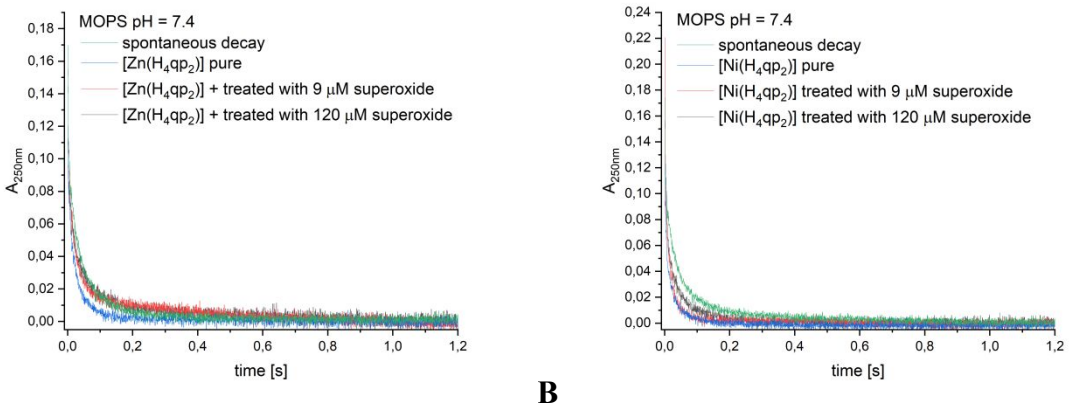

A **B**

Figure 6. Kinetic traces of superoxide decomposition at 250 nm in 60 mM MOPS buffer, pH 7.4 for H_4qp2 complexes after pre-treatment with either 9 or 120 μM KO_2. A) Data for $[Zn^{II}(H_4qp2)](OTf)_2$. B) Data for **2**.

EPR Analysis of Viable Intermediates for SOD Mimicry

We attempted to independently generate possible intermediates relevant to the SOD mimicry by reacting **1** and **2** with stoichiometric amounts of Ag(OTf) and Et_3N in MeCN (Figure 7). We previously ran analogous studies with the Zn(II) complexes with H_2qp1 and H_4qp2 to

demonstrate that Zn(II)-quinoxyl radical species were viable intermediates in the catalytic cycles for $O_2^{\cdot-}$ dismutation.[29, 30]

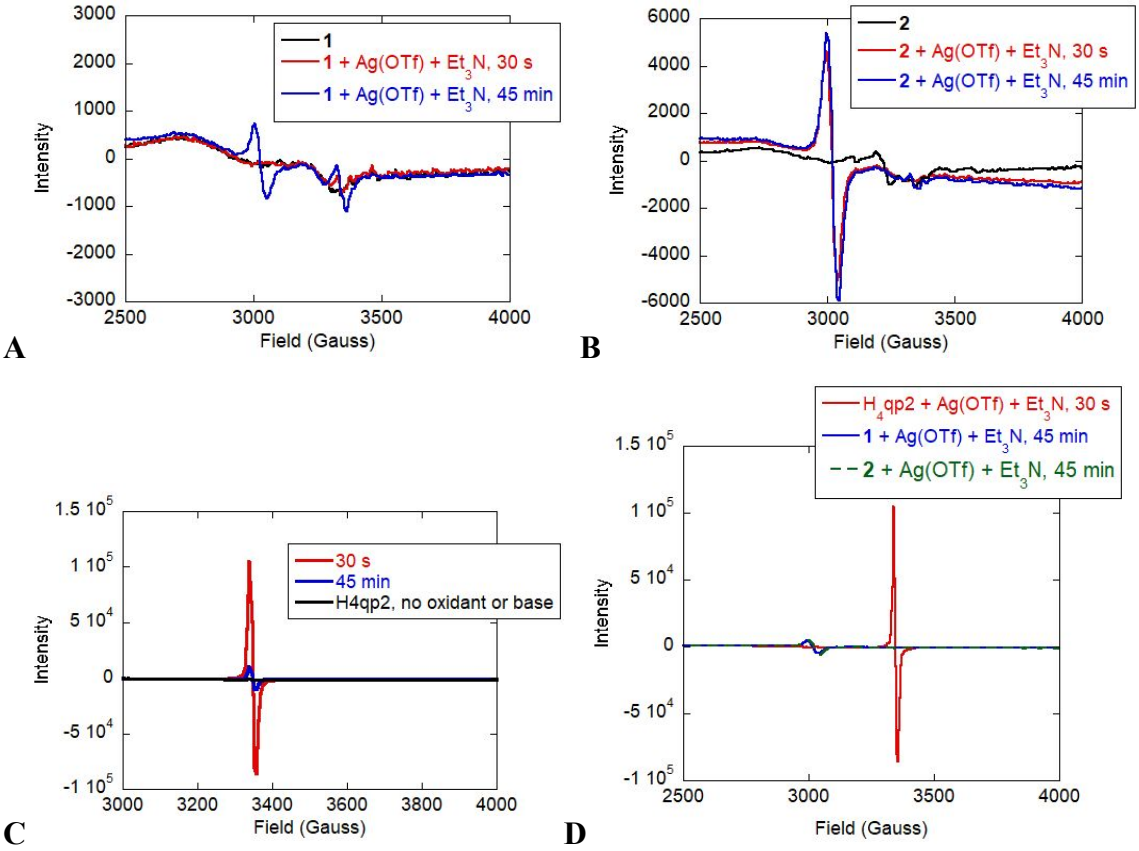

Figure 7. X-band EPR data for the reactions between A) 1.0 mM **1**, B) 1.0 mM **2**, and C) H_4qp2 with 1.0 mM Ag(OTf) and 1.0 mM Et_3N in MeCN. At the given time points, aliquots were rapidly filtered and frozen at 77 K. D) Signal intensity comparison.

EPR analysis of the reaction mixtures suggests that a small amount of the nickel has been oxidized to the +3 oxidation state for both **1** and **2**. For **1**, two small features appear with $g = 2.22$ and $g = 2.00$. The intensities of the features maximize by 45 min. The $g = 2.00$ feature resembles that found for the aforementioned Zn(II)-quinoxyl radical species and resembles features seen for previously reported Ni(II) complexes with organic radicals.[65, 66] The $g = 2.22$ feature may be consistent with a Ni(III) species,[66] although we cannot completely preclude contamination from the silver. Complex **2** gives rise to a stronger feature at $g = 2.22$ upon reaction with the Ag(I) oxidant and base. No features that can be unambiguously distinguished from noise are seen around $g = 2.00$, suggesting that organic radicals are not present above the limit of detection. The approximately ten-fold greater intensity of the $g = 2.22$ feature may suggest that the additional

quinolate in the H_4qp2 framework can stabilize Ni(III) to a greater extent than H_2qp1 since the dianionic H_2qp2^{2-} ligand would be anticipated to better neutralize a higher positive charge on the metal center. Nonetheless, the signal-to-noise for both **1** and **2** are poor, and the signal intensities are much weaker than those of the Zn(II)-quinoxyl radical species detected in our prior studies.[29, 30] Reacting an equivalent amount of H_4qp2 with Ag(OTf) and Et_3N results in a much more intense EPR signal, further demonstrating that any Ni(III) produced by these non-catalytic conditions accumulates to near negligible concentrations.

Discussion

The *N*-(2,5-dihydroxybenzyl)-*N,N',N'*-tris(2-pyridinylmethyl)-1,2-ethanediamine (H_2qp1) and *N,N'*-bis(2,5-dihydroxybenzyl)-*N,N'*-bis(2-pyridinylmethyl)-1,2-ethanediamine (H_4qp2) ligands were previously used to prepare complexes with Mn(II) and Zn(II), and precipitation from organic solvents enabled us to obtain $[Mn^{II}(H_2qp1)(MeCN)](OTf)_2$, $[Mn^{II}(H_4qp2)Br_2]$, $[Zn^{II}(H_2qp1)(OTf)](OTf)$, $[Zn^{II}(H_2qp1)(MeCN)](OTf)_2$, and $[Zn^{II}(H_4qp2)](OTf)_2$ in moderately high yields ranging from 70% to 90%.[24, 25, 29, 30] The syntheses of Ni(II) complexes with these ligands likewise proceed smoothly, and crystalline samples of both $[Ni^{II}(H_2qp)(MeCN)](OTf)_2$ (**1**) and $[Ni^{II}(H_4qp2)(MeCN)_2](OTf)_2$ (**2**) can be obtained in yields exceeding 40%.

In the crystal structures of $[Mn^{II}(H_4qp2)Br_2]$, $[Zn^{II}(H_2qp1)(OTf)](OTf)$, and $[Zn^{II}(H_2qp1)(MeCN)](OTf)_2$, which were all obtained from MeCN/ether solutions, the protonated quinols do not bind to the metal center.[25, 29] In the structures of **1** and **2**, the quinolic portions of the ligands likewise do not coordinate to the Ni(II) (Figure 1). Overall, the structural data for the Mn(II), Zn(II), and Ni(II) complexes suggest that the pyridines in the ligand are stronger ligands than the quinols. As with the aforementioned Mn(II) and Zn(II) complexes, however, the solid-state structures of **1** and **2** grown from MeCN solution do not appear to be maintained in water.[25, 29] UV/vis measurements show that at pH 7.0, a single quinol from each complex has deprotonated to a quinolate, which would have a stronger affinity for cationic metal centers. The pK_a values obtained from potentiometric pH titrations range from 5.8-7.1; these are more consistent with M(II)-phenol complexes than free phenols.[9, 23, 25, 28-30, 54, 55] The pH titration data for **1** and **2** likewise demonstrate that a quinol from each ligand has deprotonated at pH 7.0. Given that Ni(II) ions rarely have coordination numbers that exceed six,[56, 57] the major aqueous cations at this pH are likely $[Ni^{II}(Hqp1)]^+$ and $[Ni^{II}(H_3qp2)]^+$. Although the second quinol in the H_3qp2^- complex

interacts weakly with the metal center and could be displaced by water to yield $[Ni^{II}(H_3qp2)(H_2O)]^+$, our ^{17}O NMR data indicate that water molecules are not exchanging at the metal center, suggesting that water is not coordinating to the Ni(II). Although firm stability constants have not been measured for either **1** or **2** due to the lack of metal ion dissociation under acidic conditions, they are unambiguously more stable than their Mn(II) analogs, which release their metal ions under such conditions.[25, 28]

Although there is a class of superoxide dismutases (SODs) that naturally contain nickel, neither **1** nor **2** resemble these either structurally or spectroscopically. Nickel-containing SODs cycle between five-coordinate Ni(III) and four-coordinate Ni(II) species.[67] Further, the coordination spheres of the enzymes include two cysteinates and two backbone amidates, with an imidazole ligand completing the coordination of the Ni(III) form. Instead of an S_2N_3 or S_2N_2 coordination sphere, **1** and **2** have N_5O and N_4O_2 sets of donor atoms, respectively.

Despite their lack of resemblance to the active sites in nickel SODs, both **1** and **2** are nonetheless functional mimics of these enzymes. Stopped-flow kinetics analyses of the direct reactions between the Ni(II) complexes and KO_2 demonstrate that **1** and **2** are highly capable antioxidants (Figure 3, Table 4). The metal-free quinolic ligands do not display this behavior.[28, 29] The SOD mimicry exhibited by **1** and **2** is noteworthy since nickel has rarely supported this sort of reactivity in small molecule complexes. Complexes with short peptide chains, or maquettes, have been able to reproduce many of the spectroscopic features of nickel-containing SODs and much of the reactivity.[68-75] Complexes with non-peptide-derived ligands, conversely, may react stoichiometrically with superoxide but usually do not act as catalysts.[76-78] Two studies reported catalysis by nickel complexes with azo-aldehyde and Schiff base ligands.[79, 80] The reported k_{cat} values range from 1×10^6 M^{-1} s^{-1} to 8×10^6 M^{-1} s^{-1}, but it should be noted that these rate constants were determined through assays, rather than stopped-flow kinetics measurements. Duboc's group, conversely, reported a series of Ni(II) complexes with peptide-containing ligands that were demonstrated to be catalysts by stopped-flow kinetics.[75, 81-83] The most active of these compounds catalytically degraded $O_2^{\cdot-}$ with a $k_{cat} = 8.6 \times 10^6$ M^{-1} s^{-1} in 60 mM HEPES solution buffered to pH 8.1.[75] Complexes **1** and **2** are approximately 1.4 and 11 times more active, respectively, under similar conditions (Table 4), with the caveats that we use MOPS instead of HEPES as the sulfonate-derived buffer and operate at pH 7.8 rather than 8.1.

The activities of the nickel complexes, particularly that of **2**, compare well to those of manganese-containing SOD mimics.[15, 19, 20, 31, 33, 84-87] The k_{cat} measured for **2** in pH 7.4 MOPS buffer exceeds the 9.7×10^7 M^{-1} s^{-1} value measured for $[Mn^{II}(H_2qp1)(MeCN)]^{2+}$ in pH 7.4 HEPES.[28] Although it is not the most active of manganese-porphyrin SOD mimics, the well-characterized $MnBr_8TM\text{-}4\text{-}PyP^{4+}$ has a k_{cat} of 21.9×10^7 M^{-1} s^{-1}; this rate constant, however, may not be directly comparable to the other mentioned values since this k_{cat} was measured through an assay rather than stopped-flow kinetics.[88] The manganese-pentaazamacrocycle M40401 is unambiguously more active as an SOD mimic, with a $k_{cat} = 1.5 \times 10^9$ M^{-1} s^{-1} in pH 7.4 HMES buffer,[89, 90] but this complex is much less water-stable than both $[Mn^{II}(H_2qp1)(MeCN)]^{2+}$ and **2**.[28]

Another notable feature about **1** and **2** is that they only lose about 50% of their catalytic activity upon switching from a sulfonic acid-based buffer to phosphate buffer (Table 4). Many manganese complexes that have been studied in phosphate buffer, conversely, lose much more of their activity upon such a switch,[28, 31, 91, 92] and examples that retain most of their activity, such as $[Mn^{II}(H_4qp2)Br_2]$, often tend to be poorer catalysts under all studied conditions.[28, 31] The Zn(II) complexes with H_2qp1 and H_4qp2, $[Zn^{II}(H_2qp1)(OTf)]^+$ and $[Zn^{II}(H_4qp4)]^{2+}$, conversely, display enhanced SOD mimicry in phosphate buffer to the extent where they outperform their manganese analogs in this medium (Table 4).[29, 30]

That **2** is more catalytically active than **1** may be initially surprising since the Mn(II) complex with H_4qp2 is much less active than the one with H_2qp1 in HEPES solution (although the catalysts are approximately equivalent in phosphate buffer).[28] With Mn(II), the ligands fully deprotonate to $Hqp1^-$ and H_2qp2^{2-}, rendering their complexes monocationic and neutral, respectively. Higher positive charges on SOD mimics tend to lead to faster catalysis, explaining the higher k_{cat} for the H_2qp1 complex. With Ni(II), conversely, the H_4qp2 does not fully deprotonate under catalytic conditions; consequently, both **1** and **2** form predominantly monocationic species in water between pH 7 and 7.8.

Although the Ni(II) complex with H_2qp1 is approximately half as active as its Zn(II) analog in phosphate buffer based on their k_{cat} values, the Ni(II) complex with H_4qp2 is over twice as active as $[Zn^{II}(H_4qp2)]^{2+}$ under such conditions (Table 4). Complex **2** appears to be much more stable than both **1** (Figures S19-S22) and the Zn(II) complexes. The reaction between **2** and KO_2 does not promote metal ion dissociation from the oxidized forms of H_4qp2 as it does with $[Zn^{II}(H_4qp2)]^{2+}$,[30] and samples of **2** that have previously reacted with $O_2^{\cdot-}$ can be used to catalyze

subsequent superoxide degradation reactions (Figure 6). The greater *operando* stability of **2** likely explains its higher activity.

Phosphate is generally believed to inhibit SOD mimetics by acting as a competitive inhibitor that blocks the coordination of $O_2^{\cdot-}$ to the metal center. A recent computational analysis from our groups suggests that phosphate binds to M(III) ions much more tightly than to M(II) ions.[93] Manganese can readily access the +3 oxidation state;[57] consequently, phosphate inhibition has been observed to be particularly severe for manganese-catalyzed superoxide dismutation.[28, 31] Zinc, conversely, cannot access the +3 oxidation state, and phosphate actually enhances, rather than hampers, zinc-catalyzed $O_2^{\cdot-}$ dismutation due to its ability to more efficiently transfer protons to and from the positively charged species on the catalytic cycle.[29, 30] The redox activity of nickel of intermediary to those of manganese and zinc. Although Ni(III) is relevant to the activities of Ni SODs, Ni(III) species are not observed during catalysis.[57] Even though we could use Ag(OTf) to oxidize trace portions of samples of **1** and **2** to what may be Ni(III) species (Figure 7), we do not observe any Ni(III) complexes in samples of **1** and **2** oxidized by KO_2 in our cryo-MS experiments (Figure 4), nor can we access Ni(III) by CV (Figure 2). If the $O_2^{\cdot-}$ reactions oxidize the metal center to Ni(III) under catalytic conditions, such species would have to be extremely short-lived. Although it was initially tempting to attribute the partial phosphate inhibition of **1** and **2** to the anions' coordination to Ni(III) metal centers, our evidence suggests that these higher-valent metal centers are not abundant enough during catalysis to have an impact. Consequently, the rationale for why phosphate only partly inhibits nickel-driven SOD mimicry remains unclear.

Mechanistically, the SOD mimicry exhibited by **1** and **2** appears to more strongly resemble that of their Zn(II) analogs.[29, 30] Even though a prior report found that Ni(III) complexes could directly oxidize quinols,[94] our CSI-MS and UV/vis results suggest that the SOD catalysis for **1** and **2** primarily involves changes to the oxidation states of the ligands rather than the metal center. This differs markedly from what was observed for $[Mn^{II}(H_2qp1)]^{2+}$ and $[Mn^{II}(H_4qp2)]^{2+}$, which proceed through M(III) and M(IV) species during catalysis.[28] The MS data show that the quinols within the ligands oxidize to *para*-quinones. Our MS results also suggest that the *para*-quinones can continue to reduce back to quinols even after other portions of the ligand begin to get oxidized. The oxidation state of the nickel in all species identified by either MS or CSI-MSI is +2. Although traces of Ni(III) may form with a different oxidant (Figure 7), we do not observe any Ni(III) species in the $O_2^{\cdot-}$ reactions even with H_4qp2, which was found to support the +3 and even the +4 oxidation

state for manganese under similar conditions.[28] The cryo-MS and UV/vis data are consistent with the formation of metal complexes with semiquinone radicals (Figure 4, Figure 5); analogous intermediates were previously observed in the SOD mimicry with manganese and zinc complexes with these ligands.[28, 30]

The lack of rapid water molecule exchange for **1** and **2** further differentiates these compounds from their manganese analogs.[25, 28] That the Ni(II) centers are coordinatively saturated at the beginning of the catalysis may suggest that the initial reactions with superoxide are outer-sphere. With the more labile manganese H_2qp1 and H_4qp2 complexes, cryo-MS detected intermediates that are consistent with inner-sphere reactions with O.[28] $[Zn^{II}(H_2qp1)]^{2+}$ was also proposed to reduce and oxidize $O_2^{\cdot-}$ through inner-sphere pathways, albeit on the basis of calculations.[93] Although cryo-MS did not detect intermediates that could be assigned as nickel-superoxide adducts, further studies are needed to determine the relevance of inner- and outer-sphere pathways for $O_2^{\cdot-}$ reduction and oxidation and more fully elucidate the mechanism.

Conclusions

We find that polydentate ligands with redox-active quinols can enable nickel to catalytically degrade superoxide at rates that are highly competitive with those of the most active reported manganese-containing SOD mimics. Although phosphate inhibits catalysis, the diminishment in activity is not as severe as seen for other similarly high performing antioxidants. The ligand design has a noticeable impact on the reactivity in that the complex with the second quinol is much more active. The catalytic cycle remains under investigation but likely involves primarily ligand-centered redox cycles and possibly outer-sphere pathways for at least some of the individual reactions. Overall, the nickel-containing catalysts more strongly resemble their zinc-containing analogs than their manganese-containing counterparts but are more robust than either.

References

1 M. I. Ahmed, J. D. Gladden, S. H. Litovsky, S. G. Lloyd, H. Gupta, S. Inusah, T. Denney, Jr., P. Powell, D. C. McGiffin, L. J. Dell'Italia, Increased Oxidative Stress and Cardiomyocyte Myofibrillar Degeneration in Patients with Chronic Isolated Mitral Regurgitation and Ejection Fraction >60%, *J. Am. Coll. Cardiol.*, **2010**, *55* (7), 671-679.

2 I. M. Fearon, S. P. Faux, Oxidative Stress and Cardiovascular Disease: Novel Tools Give (Free) Radical Insight, *J. Mol. Cell. Cardiol.*, **2009**, *47* (3), 372-381.

3 G. Eskici, P. H. Axelsen, Copper and Oxidative Stress in the Pathogenesis of Alzheimer's Disease, *Biochemistry*, **2012**, *51* (32), 6289-6311.
4 V. L. Kinnula, Production and Degradation of Oxygen Metabolites During Inflammatory States in the Human Lung, *Curr. Drug Targets. Inflamm. Allergy*, **2005**, *4* (4), 465-470.
5 S. F. AbdulSalam, F. S. Thowfeik, E. J. Merino, Excessive Reactive Oxygen Species and Exotic DNA Lesions as an Exploitable Liability, *Biochemistry*, **2016**, *55* (38), 5341-5352.
6 Q. N. Do, J. S. Ratnakar, Z. Kovács, A. D. Sherry, Redox- and Hypoxia-Responsive MRI Contrast Agents, *ChemMedChem*, **2014**, *9* (6), 1116-1129.
7 Z. Lou, P. Li, K. Han, Redox-Responsive Fluorescent Probes with Different Design Strategies, *Acc. Chem. Res.*, **2015**, *48* (5), 1358-1368.
8 G. S. Loving, S. Mukherjee, P. Caravan, Redox-Activated Manganese-Based MR Contrast Agent, *J. Am. Chem. Soc.*, **2013**, *135* (12), 4620-4623.
9 E. M. Gale, S. Mukherjee, C. Liu, G. S. Loving, P. Caravan, Structure-Redox-Relaxivity Relationships for Redox Responsive Manganese-Based Magnetic Resonance Imaging Probes, *Inorg. Chem.*, **2014**, *53* (19), 10748-10761.
10 E. M. Gale, C. M. Jones, I. Ramsay, C. T. Farrar, P. Caravan, A Janus Chelator Enables Biochemically Responsive MRI Contrast with Exceptional Dynamic Range, *J. Am. Chem. Soc.*, **2016**, *138* (49), 15861-15864.
11 B. Song, Y. Wu, M. Yu, P. Zhao, C. Zhou, G. E. Kiefer, A. D. Sherry, A Europium(III)-Based PARACEST Agent for Sensing Singlet Oxygen by MRI, *Dalton Trans.*, **2013**, *42* (22), 8066-8069.
12 S. J. Ratnakar, S. Viswanathan, Z. Kovacs, A. K. Jindal, K. N. Green, A. D. Sherry, Europium(III) DOTA-tetraamide Complexes as Redox-Active MRI Sensors, *J. Am. Chem. Soc.*, **2012**, *134* (13), 5798-5800.
13 P. B. Tsitovich, J. A. Spernyak, J. R. Morrow, A Redox-Activated MRI Contrast Agent that Switches Between Paramagnetic and Diamagnetic States, *Angew. Chem. Int. Ed.*, **2013**, *52* (52), 13997-14000.
14 P. B. Tsitovich, P. J. Burns, A. M. McKay, J. R. Morrow, Redox-Activated MRI Contrast Agents Based on Lanthanide and Transition Metal Ions, *J. Inorg. Biochem.*, **2014**, *133*, 143-154.
15 D. P. Riley, R. H. Weiss, Manganese Macrocyclic Ligand Complexes as Mimics of Superoxide Dismutase, *J. Am. Chem. Soc.*, **1994**, *116* (1), 387-388.
16 D. P. Riley, P. J. Lennon, W. L. Neumann, R. H. Weiss, Toward the Rational Design of Superoxide Dismutase Mimics: Mechanistic Studies for the Elucidation of Substituent Effects on the Catalytic Activity of Macrocyclic Manganese(II) Complexes, *J. Am. Chem. Soc.*, **1997**, *119* (28), 6522-6528.
17 A. Tovmasyan, S. Carballal, R. Ghazaryan, L. Melikyan, T. Weitner, C. G. C. Maia, J. S. Reboucas, R. Radi, I. Spasojevic, L. Benov, I. Batinic-Haberle, Rational Design of Superoxide Dismutase (SOD) Mimics: The Evaluation of the Therapeutic Potential of New Cationic Mn Porphyrins with Linear and Cyclic Substituents, *Inorg. Chem.*, **2014**, *53* (21), 11467-11483.
18 I. A. Abreu, D. E. Cabelli, Superoxide Dismutases- A Review of the Metal-Associated Mechanistic Variations, *Biochim. Biophys. Acta*, **2010**, *1804*, 263-274.
19 D. P. Riley, Functional Mimics of Superoxide Dismutase Enzymes as Therapeutic Agents, *Chem. Rev.*, **1999**, *99* (9), 2573-2588.
20 I. Batinic-Haberle, J. S. Reboucas, I. Spasojevic, Superoxide Dismutase Mimics: Chemistry, Pharmacology, and Therapeutic Potential, *Antioxid. Redox Signal.*, **2010**, *13*, 877-918.

21 I. Batinic-Haberle, Z. Rajic, A. Tovmasyan, J. S. Reboucas, X. Ye, K. W. Leong, M. W. Dewhirst, Z. Vujaskovic, L. Benov, I. Spasojevic, Diverse Functions of Cationic Mn(III) N-substituted Pyridylporphyrins, Recognized as SOD Mimics, *Free Rad. Biol. Med.*, **2011**, *51*, 1035-1053.
22 M. Yu, R. J. Beyers, J. D. Gorden, J. N. Cross, C. R. Goldsmith, A Magnetic Resonance Imaging Contrast Agent Capable of Detecting Hydrogen Peroxide, *Inorg. Chem.*, **2012**, *51*, 9153-9155.
23 S. Karbalaei, E. Knecht, A. Franke, A. Zahl, A. C. Saunders, P. R. Pokkuluri, R. J. Beyers, I. Ivanović-Burmazović, C. R. Goldsmith, A Macrocyclic Ligand Framework That Improves Both the Stability and T_1-Weighted MRI Response of Quinol-Containing H_2O_2 Sensors, *Inorg. Chem.*, **2021**, *60* (12), 8368-8379.
24 M. Yu, S. L. Ambrose, Z. L. Whaley, S. Fan, J. D. Gorden, R. J. Beyers, D. D. Schwartz, C. R. Goldsmith, A Mononuclear Manganese(II) Complex Demonstrates a Strategy to Simultaneously Image and Treat Oxidative Stress, *J. Am. Chem. Soc.*, **2014**, *136*, 12836-12839.
25 M. Yu, M. B. Ward, A. Franke, S. L. Ambrose, Z. L. Whaley, T. M. Bradford, J. D. Gorden, R. J. Beyers, R. C. Cattley, I. Ivanović-Burmazović, D. D. Schwartz, C. R. Goldsmith, Adding a Second Quinol to a Redox-Responsive MRI Contrast Agent Improves Its Relaxivity Response to H_2O_2, *Inorg. Chem.*, **2017**, *56* (5), 2812-2826.
26 O. Iranzo, Manganese Complexes Displaying Superoxide Dismutase Activity: A Balance between Different Factors, *Bioorg. Chem.*, **2011**, *39*, 73-87.
27 J. M. McCord, I. Fridovich, Superoxide Dismutase: An Enzymic Function for Erythrocuprein (Hemocuprein), *J. Biol. Chem.*, **1969**, *244* (22), 6049-6055.
28 L. Senft, J. L. Moore, A. Franke, K. R. Fisher, A. Scheitler, A. Zahl, R. Puchta, D. Fehn, S. Ison, S. Sader, I. Ivanović-Burmazović, C. R. Goldsmith, Quinol-Containing Ligands Enable High Superoxide Dismutase Activity by Modulating Coordination Number, Charge, Oxidation States and Stability of Manganese Complexes throughout Redox Cycling, *Chem. Sci.*, **2021**, *12* (31), 10483-10500.
29 M. B. Ward, A. Scheitler, M. Yu, L. Senft, A. S. Zillmann, J. D. Gorden, D. D. Schwartz, I. Ivanović-Burmazović, C. R. Goldsmith, Superoxide Dismutase Activity Enabled by a Redox-Active Ligand rather than a Metal, *Nature Chem.*, **2018**, *10* (12), 1207-1212.
30 J. L. Moore, J. Oppelt, L. Senft, A. Franke, A. Scheitler, M. W. Dukes, H. B. Alix, A. C. Saunders, S. Karbalaei, D. D. Schwartz, I. Ivanović-Burmazović, C. R. Goldsmith, Diquinol Functionality Boosts the Superoxide Dismutase Mimicry of a Zn(II) Complex with a Redox-Active Ligand while Maintaining Catalyst Stability and Enhanced Activity in Phosphate Solution, *Inorg. Chem.*, **2022**, *61* (49), 19983-19997.
31 F. C. Friedel, D. Lieb, I. Ivanović-Burmazović, Comparative Studies on Manganese-Based SOD Mimetics, Including the Phosphate Effect, by Using Global Spectral Analysis, *J. Inorg. Biochem.*, **2012**, *109*, 26-32.
32 D. Lieb, F. C. Friedel, M. Yawer, A. Zahl, M. M. Khusniyarov, F. W. Heinemann, I. Ivanović-Burmazović, Dinuclear Seven-Coordinate Mn(II) Complexes: Effect of Manganese(II)-Hydroxo Species on Water Exchange and Superoxide Dismutase Activity, *Inorg. Chem.*, **2013**, *52* (1), 222-236.
33 I. Kenkel, A. Franke, M. Dürr, A. Zahl, C. Dücker-Benfer, J. Langer, M. R. Filipović, M. Yu, R. Puchta, S. R. Fiedler, M. P. Shores, C. R. Goldsmith, I. Ivanović-Burmazović, Switching between Inner- and Outer-Sphere PCET Mechanisms of Small Molecule Activation:

Superoxide Dismutation and Oxygen/Superoxide Reduction Reactivity Deriving from the Same Manganese Complex, *J. Am. Chem. Soc.*, **2017**, *139* (4), 1472-1484.
34 C. Bergwitz, H. Jüppner, Phosphate Sensing, *Adv. Chronic Kidney Dis.*, **2011**, *18* (2), 132-144.
35 A. Bevington, K. I. Mundy, A. J. Yates, J. A. Kanis, R. G. Russell, D. J. Taylor, B. Rajagopalan, G. K. Radda, A Study of Intracellular Orthophosphate Concentration in Human Muscle and Erythrocytes by ^{31}P Nuclear Magnetic Resonance Spectroscopy and Selective Chemical Assay, *Clin. Sci.*, **1986**, *71* (6), 729-735.
36 A. E. Martell, *Critical Stability Constants*; Plenum Press, 1974.
37 H. Irving, R. J. P. Williams, The Stability of Transition-Metal Complexes, *J. Chem. Soc.*, **1953**, (0), 3192-3210.
38 P. Chen, S. Chakraborty, S. Mukhopadhyay, E. Lee, M. M. B. Paoliello, A. B. Bowman, M. Aschner, Manganese Homeostasis in the Nervous System, *J. Neurochem.*, **2015**, *134* (4), 601-610.
39 B. Drahoš, I. Lukeš, É. Tóth, Manganese(II) Complexes as Potential Contrast Agents for MRI, *Eur. J. Inorg. Chem.*, **2012**, *2012* (12), 1975-1986.
40 J. B. Aitken, E. L. Shearer, N. M. Giles, B. Lai, S. Vogt, J. S. Reboucas, I. Batinic-Haberle, P. A. Lay, G. I. Giles, Intracellular Targeting and Pharmacological Activity of the Superoxide Dismutase Mimics MnTE-2-PyP^{5+} and MnTnHex-2-PyP^{5+} Regulated by Their Porphyrin Ring Substituents, *Inorg. Chem.*, **2013**, *52*, 4121-4123.
41 P. C. M. van Zijl, N. N. Yadav, Chemical Exchange Saturation Transter (CEST): What is in a Name and What Isn't?, *Magn. Reson. Med.*, **2011**, *65*, 927-948.
42 S. Zhang, M. Merritt, D. E. Woessner, D. E. Lenkinski, A. D. Sherry, PARACEST Agents: Modulating MRI Contrast via Water Proton Exchange, *Acc. Chem. Res.*, **2003**, *36* (10), 783-790.
43 P. Gans, A. Sabatini, A. Vacca, *Talanta*, **1996**, *43*, 1739-1753.
44 S. B. Kedare, R. P. Singh, Genesis and Development of DPPH Method of Antioxidant Assay, *J. Food Sci. Technol.*, **2011**, *48* (4), 412-422.
45 M. S. Blois, Antioxidant Determinations by Use of a Stable Free Radical, *Nature*, **1958**, *181*, 1199-1200.
46 E. R. Milaeva, D. B. Shpakovsky, Y. A. Gracheva, S. I. Orlova, V. V. Maduar, B. N. Tarasevich, N. N. Meleshonkova, L. G. Dubova, E. F. Shevtsova, Metal Complexes with Functionalised 2,2'-Dipicolylamine Ligand Containing an Antioxidant 2,6-Di-*tert*-butylphenol Moiety: Synthesis and Biological Studies, *Dalton Trans.*, **2013**, *42* (19), 6817-6828.
47 R. S. Drago, *Physical Methods for Chemists*; Surfside Scientific Publishers, 1992.
48 S. V. Obisesan, C. Rose, B. H. Farnum, C. R. Goldsmith, Co(II) Complex with a Covalently Attached Pendent Quinol Selectively Reduces O_2 to H_2O, *J. Am. Chem. Soc.*, **2022**, *144* (50), 22826-22830.
49 S. Karbalaei, A. Franke, A. Jordan, C. Rose, P. R. Pokkuluri, R. J. Beyers, A. Zahl, I. Ivanović-Burmazović, C. R. Goldsmith, A Highly Water- and Air-Stable Iron-Containing MRI Contrast Agent Sensor for H_2O_2, *Chem. Eur. J.*, **2022**, *28*, e202201179.
50 S. Karbalaei, A. Franke, J. Oppelt, T. Aziz, A. Jordan, P. R. Pokkuluri, D. D. Schwartz, I. Ivanović-Burmazović, C. R. Goldsmith, A Macrocyclic Quinol-Containing Ligand Enables High Catalase Activity even with a Redox-Inactive Metal at the Expense of the Ability to Mimic Superoxide Dismutase, *Chem. Sci.*, **2023**, *14*, 9910-9922.
51 R. D. Shannon, Revised Effective Ionic Radii and Systematic Studies of Interatomic Distances in Halides and Chalcogenides, *Acta Cryst.*, **1976**, *A32*, 751-767.

52 T.-L. Chan, T. C. W. Mak, X-Ray Crystallographic Study of Guest-Molecule Orientations in the β-Hydroquinone Clathrates of Acetonitrile and Methyl Isocyanide, *J. Chem. Soc., Perkin Trans. 2*, **1983**, (6), 777-781.
53 M. Quan, D. Sanchez, M. F. Wasylkiw, D. K. Smith, Voltammetry of Quinones in Unbuffered Aqueous Solution: Reassessing the Roles of Proton Transfer and Hydrogen Bonding in the Aqueous Electrochemistry of Quinones, *J. Am. Chem. Soc.*, **2007**, *129* (42), 12847-12856.
54 S. C. Sahoo, M. Dubey, M. A. Alam, M. Ray, Effect of Metal Coordination and Intra-Molecular H-Bond on the Acidity of Phenolic Proton in a Set of Structurally Characterized Octahedral Ni(II) Complexes of l-Histidine Derivative, *Inorg. Chim. Acta*, **2010**, *363* (12), 3055-3060.
55 Y. Iitaka, T. Koike, E. Kimura, Molecular Structure of a Nickel(II) Complex with Phenolate Appended Cyclam, *Inorg. Chem.*, **1986**, *25* (4), 402-404.
56 D. Casanova, P. Alemany, J. M. Bofill, S. Alvarez, Shape and Symmetry of Heptacoordinate Transition-Metal Complexes: Structural Trends, *Chem. Eur. J.*, **2003**, *9* (6), 1281-1295.
57 F. A. Cotton, G. Wilkinson, *Advanced Inorganic Chemistry*; John Wiley & Sons, 1988.
58 J. Ancerewicz, E. Migliavacca, P.-A. Carrupt, B. Testa, F. Brée, R. Zini, J.-P. Tillement, S. Labidalle, D. Guyot, A.-M. Chauvet-Monges, A. Crevat, A. Le Ridant, Structure-Property Relationships of Trimetazidine Derivatives and Model Compounds as Potential Antioxidants, *Free Rad. Biol. Med.*, **1998**, *25* (1), 113-120.
59 I. Fridovich, Superoxide Anion Radical (O_2^-), Superoxide Dismutases, and Related Matters, *J. Biol. Chem.*, **1997**, *272* (30), 18515-18517.
60 S. I. Liochev, Superoxide Dismutase Mimics, Other Mimics, Antioxidants, Prooxidants, and Related Matters, *Chem. Res. Toxicol.*, **2013**, *26*, 1312-1319.
61 D. P. Riley, W. J. Rivers, R. H. Weiss, Stopped-Flow Kinetic Analysis for Monitoring Superoxide Decay in Aqueous Systems, *Anal. Biochem.*, **1991**, *196*, 344-349.
62 S. I. Liochev, I. Fridovich, Lucigenin (Bis-N-methylacridinium) as a Mediator of Superoxide Anion Production, *Arch. Biochem. Biophys.*, **1997**, *337*, 115-120.
63 A. J. Swallow, In *Functions of Quinones in Energy Converting Systems*, Trumpower, B. L. Ed.; Elsevier, Inc., 1982; pp 59-72.
64 X. Zhao, H. Imahori, C.-G. Zhan, Y. Sakata, S. Iwata, T. Kitagawa, Resonance Raman and FTIR Spectra of Isotope-Labeled Reduced 1,4-Benzoquinone and Its Protonated Forms in Solutions, *J. Phys. Chem. A*, **1997**, *101* (4), 622-631.
65 T. D. Manuel, J.-U. Rohde, Reaction of a Redox-Active Ligand Complex of Nickel with Dioxygen Probes Ligand-Radical Character, *J. Am. Chem. Soc.*, **2009**, *131* (43), 15582-15583.
66 R. Kunert, C. Philouze, O. Jarjayes, F. Thomas, Stable M(II)-Radicals and Nickel(III) Complexes of a Bis(phenol) N-Heterocyclic Carbene Chelated to Group 10 Metal Ions, *Inorg. Chem.*, **2019**, *58* (12), 8030-8044.
67 D. P. Barondeau, C. J. Kassmann, C. K. Bruns, J. A. Tainer, E. D. Getzoff, Nickel Superoxide Dismutase Structure and Mechanism, *Biochemistry*, **2004**, *43* (25), 8038-8047.
68 J. Shearer, Insight into the Structure and Mechanism of Nickel-Containing Superoxide Dismutase Derived from Peptide-Based Mimics, *Acc. Chem. Res.*, **2014**, *47* (8), 2332-2341.
69 J. Shearer, L. M. Long, A Nickel Superoxide Dismutase Maquette That Reproduces the Spectroscopic and Functional Properties of the Metalloenzyme, *Inorg. Chem.*, **2006**, *45* (6), 2358-2360.
70 M. Schmidt, S. Zahn, M. Carella, O. Ohlenschläger, M. Görlach, E. Kothe, J. Weston, Solution Structure of a Functional Biomimetic and Mechanistic Implications for Nickel Superoxide Dismutases, *ChemBioChem*, **2008**, *9* (13), 2135-2146.

71 M. E. Krause, A. M. Glass, T. A. Jackson, J. S. Laurence, Novel Tripeptide Model of Nickel Superoxide Dismutase, *Inorg. Chem.*, **2010**, *49* (2), 362-364.
72 M. E. Krause, A. M. Glass, T. A. Jackson, J. S. Laurence, Embedding the Ni-SOD Mimetic Ni-NCC within a Polypeptide Sequence Alters the Specificity of the Reaction Pathway, *Inorg. Chem.*, **2013**, *52* (1), 77-83.
73 J. Shearer, Use of a Metallopeptide-Based Mimic Provides Evidence for a Proton-Coupled Electron-Transfer Mechanism for Superoxide Reduction by Nickel-Containing Superoxide Dismutase, *Angew. Chem. Int. Ed.*, **2013**, *52* (9), 2569-2572.
74 J. Shearer, K. P. Neupane, P. E. Callan, Metallopeptide Based Mimics with Substituted Histidines Approximate a Key Hydrogen Bonding Network in the Metalloenzyme Nickel Superoxide Dismutase, *Inorg. Chem.*, **2009**, *48* (22), 10560-10571.
75 P. Guinard, S. Hostachy, L. Diebold, J. Pécaut, A. Le Goff, C. Duboc, P. Delangle, Outstanding Superoxide Dismutase Catalytic Activity Of Simple Peptide-Based Nickel(II) Complexes, *Angew. Chem. Int. Ed.*, **2024**, *63* (41), e202409343.
76 S. K. Chatterjee, R. C. Maji, S. K. Barman, M. M. Olmstead, A. K. Patra, Hexacoordinate Nickel(II)/(III) Complexes that Mimic the Catalytic Cycle of Nickel Superoxide Dismutase, *Angew. Chem. Int. Ed.*, **2014**, *53* (38), 10184-10189.
77 D. Nakane, Y. Wasada-Tsutsui, Y. Funahashi, T. Hatanaka, T. Ozawa, H. Masuda, A Novel Square-Planar Ni(II) Complex with an Amino—Carboxamido—Dithiolato-Type Ligand as an Active-Site Model of NiSOD, *Inorg. Chem.*, **2014**, *53* (13), 6512-6523.
78 V. G. Snider, E. R. Farquhar, M. Allen, A. Abu-Spetani, A. Mukherjee, Design and Reactivity of Ni-Complexes Using Pentadentate Neutral-Polypyridyl Ligands: Possible Mimics of NiSOD, *J. Inorg. Biochem.*, **2017**, *175*, 110-117.
79 R. Kose, S. A. Gungor, S. Erkan Kariper, M. Kose, M. Kurtoglu, The New O,O and N,O Type Ligands and their Cu(II) and Ni(II) Complexes: Crystal Structure, Absorption-Emission Properties and Superoxide Dismutase Mimetic Studies, *Inorg. Chim. Acta*, **2017**, *462*, 130-141.
80 H.-D. Bian, J. Wang, Y. Wei, J. Tang, F.-P. Huang, D. Yao, Q. Yu, H. Liang, Superoxide Dismutase Activity Studies of Mn(III)/Cu(II)/Ni(II) Complexes with Schiff Base Ligands, *Polyhedron*, **2015**, *90*, 147-153.
81 J. Domergue, P. Guinard, M. Douillard, J. Pécaut, S. Hostachy, O. Proux, C. Lebrun, A. Le Goff, P. Maldivi, C. Duboc, P. Delangle, A Series of Ni Complexes Based on a Versatile ATCUN-Like Tripeptide Scaffold to Decipher Key Parameters for Superoxide Dismutase Activity, *Inorg. Chem.*, **2023**, *62* (23), 8747-8760.
82 J. Domergue, P. Guinard, M. Douillard, J. Pécaut, O. Proux, C. Lebrun, A. Le Goff, P. Maldivi, P. Delangle, C. Duboc, A Bioinspired Ni^{II} Superoxide Dismutase Catalyst Designed on an ATCUN-like Binding Motif, *Inorg. Chem.*, **2021**, *60* (17), 12772-12780.
83 J. Domergue, J. Pécaut, O. Proux, C. Lebrun, C. Gateau, A. Le Goff, P. Maldivi, C. Duboc, P. Delangle, Mononuclear Ni(II) Complexes with a S_3O Coordination Sphere Based on a Tripodal Cysteine-Rich Ligand: pH Tuning of the Superoxide Dismutase Activity, *Inorg. Chem.*, **2019**, *58* (19), 12775-12785.
84 D. P. Riley, S. L. Henke, P. J. Lennon, R. H. Weiss, W. L. Neumann, W. J. Rivers, K. W. Aston, K. R. Sample, H. Rahman, C.-S. Ling, J.-J. Shieh, D. H. Busch, Synthesis, Characterization, and Stability of Manganese(II) C-Substituted 1,4,7,10,13-Pentaazacyclopentadecane Complexes Exhibiting Superoxide Dismutase Activity, *Inorg. Chem.*, **1996**, *35* (18), 5213-5231.

85 G.-F. Liu, K. Dürr, R. Puchta, F. W. Heinemann, R. van Eldik, I. Ivanović-Burmazović, Chelate Electronic Properties Control the Redox Behaviour and Superoxide Reactivity of Seven-Coordinate Manganese(II) Complexes, *Dalton Trans.*, **2009**, 6292-6295.
86 I. Batinic-Haberle, I. Spasojevic, 25 Years of Development of Mn Porphyrins — from Mimics of Superoxide Dismutase Enzymes to Thiol Signaling to Clinical Trials: The Story of Our Life in the USA, *J. Porphyr. Phthalocya.*, **2019**, *23* (11-12), 1326-1335.
87 C. Policar, Mimicking SOD, Why and How: Bio-Inspired Manganese Complexes as SOD Mimic. In *Redox-Active Therapeutics. Oxidative Stress in Applied Basic Research and Clinical Practice.*, Batinić-Haberle, I., Rebouças, J., Spasojević, I. Eds.; Springer, Cham, 2016.
88 I. Batinić-Haberle, S. I. Liochev, I. Spasojević, I. Fridovich, A Potent Superoxide Dismutase Mimic: Manganese β-Octabromo-meso-tetrakis-(N-methylpyridinium-4-yl) Porphyrin, *Arch. Biochem. Biophys.*, **1997**, *343* (2), 225-233.
89 D. Salvemini, Z.-Q. Wang, J. L. Zweier, A. Samouilov, H. Macarthur, T. P. Misko, M. G. Currie, S. Cuzzocrea, J. A. Sikorski, D. P. Riley, A Nonpeptidyl Mimic of Superoxide Dismutase with Therapeutic Activity in Rats, *Science*, **1999**, *286* (5438), 304-306.
90 K. Aston, N. Rath, A. Naik, U. Slomczynska, O. F. Schall, D. P. Riley, Computer-Aided Design (CAD) of Mn(II) Complexes: Superoxide Dismutase Mimetics with Catalytic Activity Exceeding the Native Enzyme, *Inorg. Chem.*, **2001**, *40* (8), 1779-1789.
91 D. Lieb. Mechanistic and Synthetic Approaches for Activation of Water-and Oxygen-Species by Biomimetic Systems (Containing Manganese and Cobalt). University of Erlangen-Nuremberg, 2013.
92 I. Kenkel, A. Franke, M. Dürr, A. Zahl, C. Dücker-Benfer, J. Langer, M. R. Filipović, M. Yu, R. Puchta, S. R. Fiedler, M. P. Shores, C. R. Goldsmith, I. Ivanović-Burmazović, Switching between Inner- and Outer-Sphere PCET Mechanisms of Small-Molecule Activation: Superoxide Dismutation and Oxygen/Superoxide Reduction Reactivity Deriving from the Same Manganese Complex, *J. Am. Chem. Soc.*, **2017**, *139* (4), 1472-1484.
93 E. Miliordos, J. L. Moore, S. V. Obisesan, J. Oppelt, I. Ivanović-Burmazović, C. R. Goldsmith, Computational Analysis of the Superoxide Dismutase Mimicry Exhibited by a Zinc(II) Complex with a Redox-Active Organic Ligand, *J. Phys. Chem. A*, **2024**, *128* (8), 1491-1500.
94 J. C. Brodovitch, A. McAuley, T. Oswald, Kinetics and Mechanism of the Oxidation of Hydroquinone and Catechol by $[Ni(III)cyclam]^{3+}$ in Aqueous Perchlorate Media, *Inorg. Chem.*, **1982**, *21* (9), 3442-3447.

Data Availability Statement

Data supporting this article have been included as part of the Supplementary Information. Crystallographic data for **1** and **2** have been deposited at the Cambridge Crystallographic Data Centre under 2390972 and 2390973 and can be obtained from https://www.ccdc.cam.ac.uk/.